AEDC-TR-75-82

Also AIAA paper 75-1302
[illegible]
[illegible]

TURBINE ENGINE EXHAUST NOZZLE PERFORMANCE WITH NONUNIFORM INLET FLOW

ENGINE TEST FACILITY
ARNOLD ENGINEERING DEVELOPMENT CENTER
AIR FORCE SYSTEMS COMMAND
ARNOLD AIR FORCE STATION, TENNESSEE 37389

August 1975

Final Report for Period July 1973 – June 1974

Prepared for

AIR FORCE FLIGHT DYNAMICS LABORATORY (FDMM)
WRIGHT-PATTERSON AIR FORCE BASE, OHIO 45433

NOTICES

APPROVAL STATEMENT

This technical report has been reviewed and is approved for publication.

FOR THE COMMANDER

Elton R. Thompson

ELTON R. THOMPSON
Research and Development
Division
Directorate of Technology

Robert O. Dietz

ROBERT O. DIETZ
Director of Technology

UNCLASSIFIED

REPORT DOCUMENTATION PAGE		READ INSTRUCTIONS BEFORE COMPLETING FORM
1. REPORT NUMBER AEDC-TR-75-82	2 GOVT ACCESSION NO.	3 RECIPIENT'S CATALOG NUMBER
4. TITLE (and Subtitle) TURBINE ENGINE EXHAUST NOZZLE PERFORMANCE WITH NONUNIFORM INLET FLOW		5 TYPE OF REPORT & PERIOD COVERED Final Report - July 1973 to June 1974
		6. PERFORMING ORG. REPORT NUMBER
7. AUTHOR(s) S. Wehofer and R. J. Matz ARO, Inc.		8. CONTRACT OR GRANT NUMBER(s)
9 PERFORMING ORGANIZATION NAME AND ADDRESS Arnold Engineering Development Center (DY) Arnold Air Force Station Tennessee 37389		10. PROGRAM ELEMENT, PROJECT, TASK AREA & WORK UNIT NUMBERS Program Element 65401F
11. CONTROLLING OFFICE NAME AND ADDRESS Arnold Engineering Development Center (DYFS) Arnold Air Force Station Tennessee 37389		12. REPORT DATE August 1975
		13. NUMBER OF PAGES 57
14 MONITORING AGENCY NAME & ADDRESS(if different from Controlling Office)		15 SECURITY CLASS. (of this report) UNCLASSIFIED
		15a. DECLASSIFICATION/DOWNGRADING SCHEDULE N/A

16 DISTRIBUTION STATEMENT (of this Report)

Approved for public release; distribution unlimited.

17 DISTRIBUTION STATEMENT (of the abstract entered in Block 20, if different from Report)

18 SUPPLEMENTARY NOTES

Available in DDC.

19 KEY WORDS (Continue on reverse side if necessary and identify by block number)

flow	turbojets
inlets	turbofans
engines	exhaust systems
turbines	nozzles
performance	numerical analysis

20 ABSTRACT (Continue on reverse side if necessary and identify by block number)

The internal fluid dynamic performance of various turbine engine exhaust nozzle configurations was experimentally investigated. Nine fixed-geometry exhaust nozzle models representative of contemporary turbofans operating at various power levels were evaluated with uniform inlet conditions and with radial nonuniformities in total pressure and total temperature. The test conditions are representative of both low bypass turbofan and turbojet tailpipe flows. The effects of nozzle throat lip geometry on

20. ABSTRACT (Continued)

nozzle performance were evaluated. Also, the results obtained from the experimental phase were compared with the performance predicted from a numerical analysis developed at the Arnold Engineering Development Center. The major conclusion is that nozzle performance coefficients cannot be ascribed to a given nozzle configuration without some specification of the nozzle inlet flow conditions and coefficient referencing procedures.

AFSC
Arnold AFS Tenn

PREFACE

The work reported herein was conducted by the Arnold Engineering Development Center (AEDC), Air Force Systems Command (AFSC), at the request of Flight Dynamics Laboratory (AFFDL), AFSC, Wright-Patterson Air Force Base, Ohio, under Program Element 65401F. The results were obtained by ARO, Inc. (a subsidiary of Sverdrup & Parcel and Associates, Inc.), contract operator of AEDC, AFSC, Arnold Air Force Station, Tennessee. The work was done under ARO Project Number RF442. The authors of this report were S. Wehofer and R. J. Matz, ARO, Inc. The manuscript (ARO Control No. ARO-ETF-TR-75-43) was submitted for publication on April 17, 1975.

The authors would like to express their appreciation to J. A. Laughrey and P. C. Everling, Air Force Flight Dynamics Laboratory, for supporting this effort. Acknowledgement is also made to L. Weller and W. J. Phares, ARO, Inc., for their significant contributions to the experimental and data reduction phases of these investigations.

CONTENTS

ILLUSTRATIONS

TABLES

APPENDIXES

1.0 INTRODUCTION

With the advent of the high-performance, low-bypass turbofan cycle, the engine designer was faced with the problem of matching this system with an efficient exhaust nozzle configuration. For propulsion considerations, nozzle selection requires knowledge of nozzle performance characteristics produced under actual engine operating conditions. Initially, experience accumulated with turbojets was applied to the prediction of turbofan exhaust nozzle performance. As operating experience was obtained with turbofan engines, however, significant differences between actual and predicted performance were observed at some operating conditions. Experimental measurements made in the Engine Test Facility (ETF) of the Arnold Engineering Development Center (AEDC) revealed that turbofan exhaust nozzle inlet conditions were characterized by significant radial gradients in both total temperature and velocity which were not found in turbojets. The discrepancy between measured and predicted turbofan engine performance was intuitively attributed to the influence of these flow nonuniformities on nozzle performance.

In 1969, an analytical model was developed by Wehofer and Moger (Refs. 1 and 2) to corroborate performance data obtained in the ETF test cells. This analysis confirmed the earlier supposition that nozzle inlet flow nonuniformities typical of low-bypass turbofans can produce nozzle performance coefficients which differ by several percent from uniform flow (or turbojet) results. In addition, computations with this analysis indicated that relatively small changes in convergent conical nozzle exit lip radius of curvature can also significantly affect nozzle performance providing the flow remains attached to the nozzle wall.

A literature search failed to uncover any systematic nozzle experiments which might confirm the analytically predicted effects of nozzle lip radius of curvature and nonuniform inlet conditions on nozzle performance. Of the studies reviewed, the experiments of Grey and Wilsted (Ref. 3), Mourey (Ref. 4), and Glasgow, et al., (Ref. 5) are felt to be representative of turbine engine exhaust nozzle investigations conducted prior to 1972. In all three investigations, unheated air was used as the working fluid.

Grey and Wilsted and Mourey limited their investigations to simple convergent conical nozzles; Glasgow evaluated axisymmetric convergent, convergent-divergent, ejector and plug nozzle configurations representative of variable geometry exhaust nozzles at various engine operating conditions. In all cases, the convergent conical nozzles evaluated are assumed to have sharp-edged lips (i.e., zero radius of curvature) at the throat station although this is not explicitly stated in any of the references. Grey and Wilsted and Glasgow limited their studies to nozzle thrust and discharge performance evaluations but Mourey also probed and shadowgraphed the nozzle exit flow fields.

Some evidence of the limitations in existing nozzle performance data may be noted from a comparison of results obtained by different investigators for comparable nozzles (Fig. 1). Part of the difference in nozzle discharge coefficient (Fig. 1) at comparable nozzle pressure ratios is

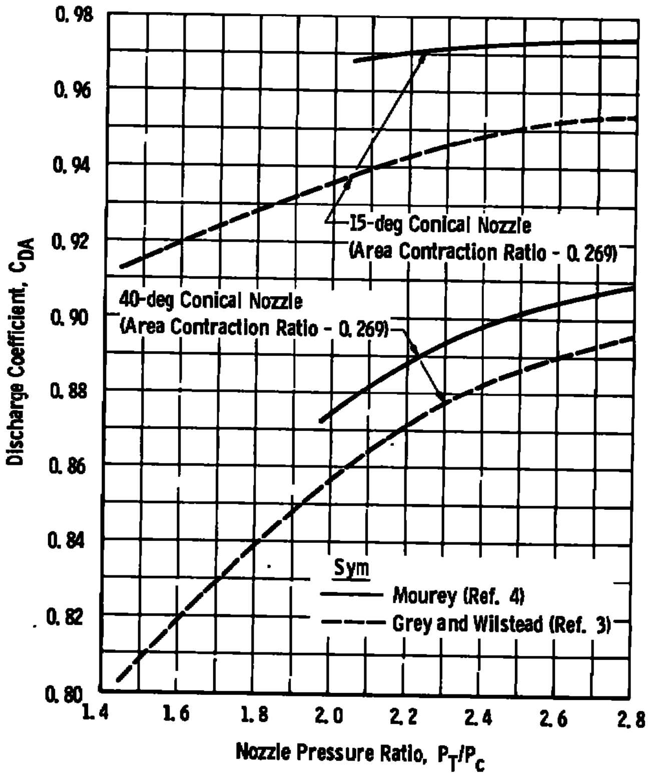

Figure 1. Conical nozzle discharge coefficient versus nozzle pressure ratio from two different test rigs.

probably due to accuracy limitations of each of the experimental rigs and the associated instrumentation. However, some of the difference is also attributable to differences in nozzle inlet velocity profiles and to the reference conditions employed in the discharge coefficient definition. For example, Mourey's test rig included a relatively short (L/D ~ 7), essentially constant diameter approach pipe which should have produced a thin boundary layer and uniform nozzle inlet velocity conditions. On the other hand, Grey and Wilsted's test apparatus consisted of a long (L/D ~ 30) approach pipe with several 90-deg bends, which, based on inlet pitot probe measurements and AEDC boundary layer calculations, produced fully developed pipe flow velocity distributions at the nozzle inlet station. Therefore, Grey and Wilsted's data reflect an additional influence of large boundary layers and nonuniform total pressure profiles on nozzle performance coefficients.

Because of the apparent lack of the information required to confirm the analytical predictions, an experimental program was undertaken at AEDC/ETF to provide performance characteristics of various turbine engine exhaust nozzle configurations with nominal flow conditions representative of low-bypass turbofan engines. Results from these experiments have been used to establish the influence of flow nonuniformities on nozzle performance and to substantiate and improve details of the Wehofer-Moger analytical model. Although the effect of nonuniform inlet conditions on nozzle performance was of primary interest, investigations were also conducted with uniform flow to provide consistent baseline data for comparative purposes.

2.0 EXPERIMENTAL PROGRAM

2.1 TEST NOZZLES

Nine fixed-geometry exhaust nozzle models (Fig. 2 and Table 1) were experimentally evaluated during the investigations. The configurations were selected (1) to be representative of contemporary turbofan exhaust nozzles, and (2) to provide a systematic investigation of the effect of nozzle exit lip geometry on convergent conical nozzle performance.

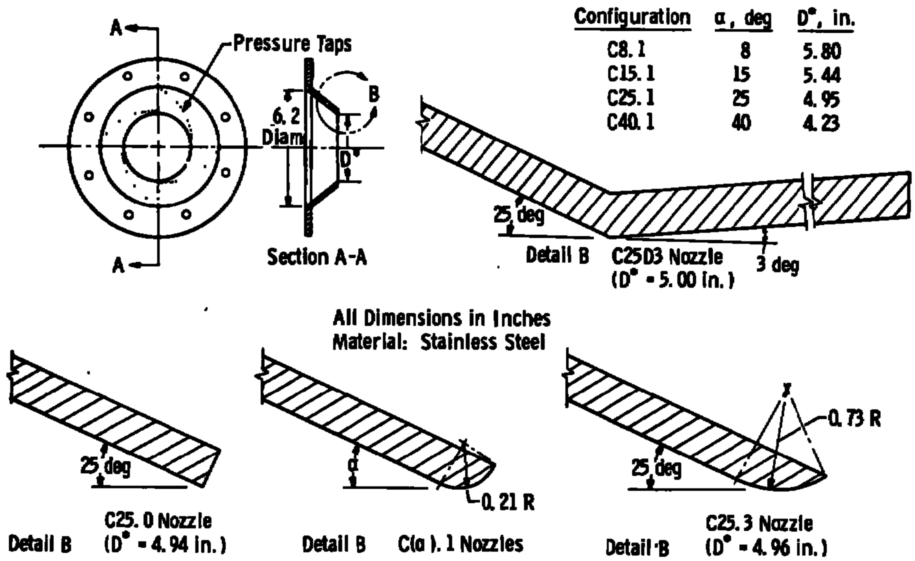

Configuration	α, deg	D*, in.
C8.1	8	5.80
C15.1	15	5.44
C25.1	25	4.95
C40.1	40	4.23

a. Schematics of conventional nozzle models

~24 scale

1.15

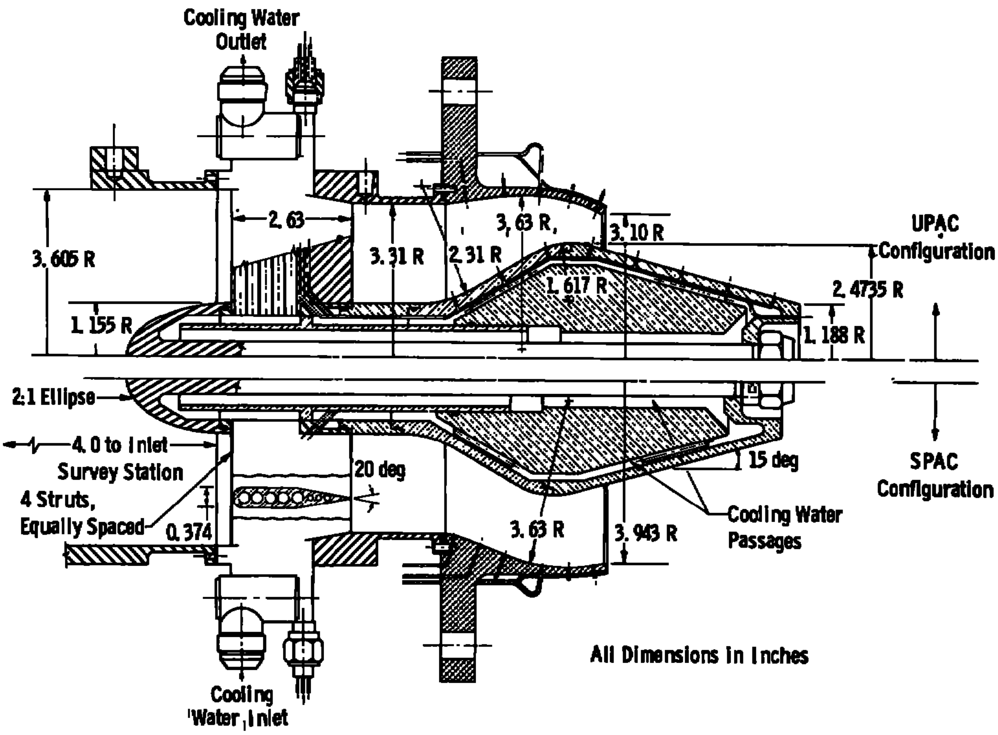

b. Schematic of plug nozzle models

Figure 2. Test nozzle design details.

$\frac{1.15}{3.31} = 0.3474$

Table 1. Summary of Exhaust Nozzles Investigated

Configuration	Nozzle Type	Nominal As-Built Geometry			
		Mean Wall Angle, deg	A_i/A^*	R_c^*	$\sim M_i)_{\gamma=1.4}$
C8.1	Conical Convergent	8.0	1.144	0.06	0.64
C15.1		15.0	1.301	0.06	0.52
C25.0		27.0	1.582	0	0.50
C25.1		25.0	1.569	0.06	0.41
C25.3		25.0	1.565	0.30	0.41
C40.1		40.5	2.149	0.07	0.28
C25D3	Convergent-Divergent	25.0 Conv. 3.4 Div.	1.538	<0.01	0.42
UPAC	Unshrouded Plug	---	3.193	---	
SPAC	Shrouded Plug	---	1.523	---	

Configurations C8.1, C15.1, C25.1, and C40.1 are representative of a variable-geometry convergent-flap primary exhaust nozzle, with a given lip geometry, operating at various power settings. Configuration C25D3 is representative of an advanced, variable-geometry, convergent-divergent exhaust nozzle in the nominal power configuration. Configurations UPAC and SPAC are representative plug exhaust nozzles and were identical, in terms of internal aerodynamic contours, to the UP_AC_1 and SP_AC_3 nozzles evaluated in the Lockheed/AFFDL integrated airframe/nozzle investigations (Ref. 5). Configurations C25.0 and C25.3 were included to provide, along with configuration C25.1, relative information on nozzle exit lip effects. All nozzles tested were dimensionally checked to establish as-built contours which differed slightly (Table 1) from the design geometries.

2.2 TEST INSTALLATION

Tests were conducted in the Propulsion Research Cell (R-1A-2) of the AEDC Engine Test Facility (ETF) (Fig. 3). Air from the von Kármán Gas Dynamics Facility (VKF), high-pressure, air supply system was used as the working fluid. The 2000- to 4000-psi air was throttled to approximately 300 psi through a pneumatically operated control valve.

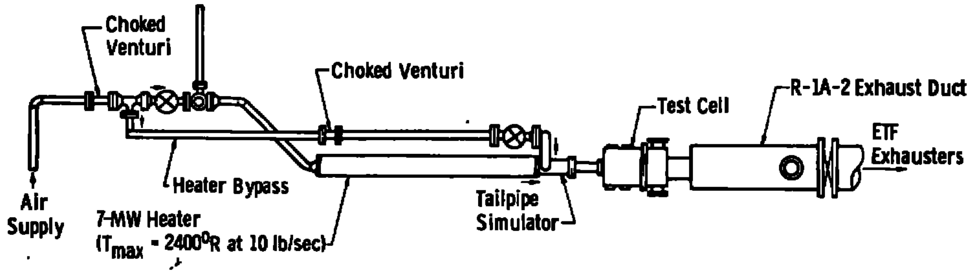

Figure 3. Propulsion nozzle research test installation.

The total airflow passing through the test nozzles was metered with a 0.95-in.-diam venturi which was designed for critical-flow operation (Ref. 6) at all test conditions. For the nonuniform inlet temperature flow investigations, the airflow was split downstream of the main metering venturi so that a portion passed through a 7-MW electrical heater which provided discharge air at temperatures up to 1100°R. Bypass air at approximately 500°R was metered with a 0.78-in.-diam venturi and then ducted radially through a manifold into a plenum section just upstream of the tailpipe simulator. Throttle valves located in the heater and bypass lines were modulated to establish the desired flow splits while maintaining critical flow in both metering venturis. Nozzle exit pressure was controlled with the ETF exhausters.

Two nozzle approach configurations (Fig. 4) were used during the investigations. The nonuniform inlet flow tests were conducted in the turbofan exhaust simulator rig (Fig. 4a), in which a core of heated air surrounded by a annulus of unheated air is provided to simulate, respectively, the turbine exhaust and bypass flow of a low-bypass turbofan. The relative length of the tailpipe simulator and the tailpipe-to-core flow pipe diameter ratio included in the rig were scaled to be representative of current technology turbofan engines. Uniform inlet flow investigations were conducted in the uniform flow test rig (Fig. 4b), in which cold air is supplied to the test nozzle through the heater line only. A relatively short approach pipe (L/D ~ 1.5) is incorporated in this installation to minimize boundary layer development upstream of the test nozzles.

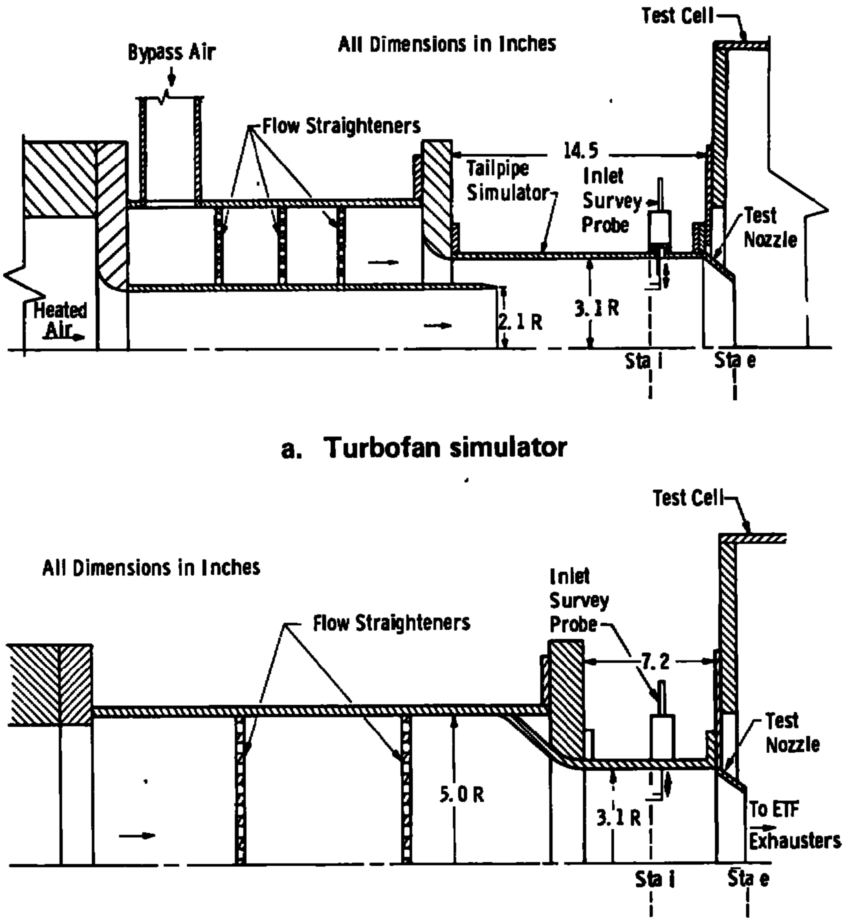

b. Uniform flow simulator

Figure 4. Nozzle approach configurations.

2.3 INSTRUMENTATION

Pressures and temperatures were measured at various points in the test nozzles, in the inlet sections, and in the venturis to establish nozzle flow characteristics at the various operating conditions. The pressure instrumentation consisted of static pressure taps installed at various points within the nozzle inlet pipes, along the internal surface of the test nozzles, in the nozzle discharge plenum, and in the metering venturis. Total pressures were also measured in the venturi inlet pipes with fixed position probes. Nozzle inlet total and static pressure and total temperature distributions were obtained with a remotely controlled, variable position survey probe (Fig. 4). The stream static pressure was determined with a calibrated 20-deg included-angle cone probe. Strain-gage-type transducers were used for the pressure measurements.

Total temperatures were measured with single-shielded, self-aspirating thermocouple probes in the venturi and test nozzle inlet pipes. Test nozzle exit and venturi throat surface temperatures were monitored with embedded thermocouples.

All data were recorded on magnetic tape through the use of an automated, sequentially sampling, millivolt-to-digital data acquisition system scanning at a rate of four parameters per second.

2.4 TEST PROCEDURE

All data were obtained at steady-state conditions. Transducers were calibrated in place before and after each test period by applying multiple pressure levels to each transducer. The applied pressure levels were measured with both a multiple-turn, fused-quartz bourdon tube and servo-controlled optical transducer and a high precision gage. Main venturi inlet pressure was continuously monitored to verify that essentially steady-state conditions were maintained throughout the data acquisition process. A random check of the venturi inlet pressure records indicated typical variations on the order of ± 0.1 to ± 0.4 percent during the time required to complete a data scan.

Test nozzle inlet pressure was nominally 10 to 20 psia in all cases. Nozzle inlet temperature was nominally 480 to 510°R for the cold flow investigations and for the bypass stream in the nonuniform temperature tests. Core temperatures for the nonuniform temperature experiments ranged from 800 to 1100°R.

3.0 DATA REDUCTION PROCEDURES

The bulk of the nozzle data in this report is presented in the form of nozzle performance coefficients. Nozzle coefficients were selected for presentation because of their traditional importance (1) in the turbine engine development cycle, (2) in the estimation of component and integrated engine performance at points in the flight envelope not included in the development test programs, and (3) in ground-to-flight test evaluations. Nozzle performance coefficients (discharge and thrust) are defined as either the ratio of engine mass flow or gross thrust to a corresponding reference condition. The generally accepted nozzle performance coefficient definitions are:

Discharge Coefficient

$$C_D = \frac{W_a}{W_{1\text{-}D}} \tag{1}$$

where, for subsonic flow

extra g

$$W_{1\text{-}D} = \frac{P_T}{\sqrt{T_T}} A^* \sqrt{\frac{2\gamma g}{R(\gamma - 1)} \left[\left(\frac{P_T}{P^*}\right)^{-\frac{2}{\gamma}} - \left(\frac{P_T}{P^*}\right)^{-\frac{\gamma+1}{\gamma}} \right]} \tag{1a}$$

ft/sec²

ft#/#°R

and for sonic and supersonic flow

$$W_{1\text{-}D} = \frac{P_T}{\sqrt{T_T}} A^* \sqrt{\frac{\gamma g}{R} \left(\frac{2}{\gamma + 1}\right)^{\frac{\gamma-1}{\gamma-1}}} \tag{1b}$$

g = gc = 32.174 ft/sec²

Thrust Coefficient

$$C_F = \frac{F_a}{F_{ideal}} \tag{2}$$

where

$$F_{ideal} = W_a \sqrt{\frac{2\gamma g}{(\gamma - 1)} RT_T \left[1 - \left(\frac{P_c}{P_T}\right)^{\frac{\gamma-1}{\gamma}} \right]} \tag{2a}$$

The reference conditions for Eqs. (1) and (2) are based on ideal, one-dimensional flow. For uniform nozzle flow (i.e., no gradients in stagnation pressure or temperature) exhausting into a quiescent environment, evaluation of the referencing conditions for Eqs. (1) and (2) is unique. For nonuniform flow (i.e., radial gradients in either stagnation pressure or temperature), the stagnation properties to be used in defining the one-dimensional reference condition become a matter of definition. As a result of these flow nonuniformities, several different referencing conditions have been used in defining turbofan exhaust nozzle performance coefficients. This inconsistency in definition makes it difficult to compare different turbofan engine thrust performance data.

An ideal reference definition would produce coefficients that are independent of nozzle flow nonuniformities; however, no reference flow definition suggested to date has demonstrated this capability for a large range in flow distortions. There are basically three different reference flow conditions that are generally employed for nonuniform flows, (1) area-weighted reference conditions, (2) stream tube reference conditions, and (3) mass-weighted reference conditions. The area-weighted and stream tube reference conditions are discussed in this report. The mass-weighted referencing procedure (Ref. 6) uses mass-weighted total pressure and temperature for the primary and bypass flow and an ideal primary and bypass thrust. However, in the present experiments, the pressure and temperature profiles at the core nozzle exit plane were not measured; therefore, mass-weighted coefficients were not calculated. In addition to these three referencing procedures, there are also variations for two stream flows such as the inclusion of "mixing-efficiency" (Ref. 7), "adder" factors (Ref. 8), or using maximized weight flow relations in place of sonic reference flow conditions (Ref. 9).

3.1 DISCHARGE COEFFICIENT

3.1.1 Area-Weighted Method

The area-weighted discharge coefficient is defined as

$$C_{DA} = \frac{W_a}{W^A_{I-D}} \tag{3}$$

The reference mass flow ($W^A{}_{1-D}$) is based on sonic flow using an area-weighted average total pressure and temperature outside the boundary layer;

$$W^A_{1\text{-}D} = \frac{P^A_T A^*}{\sqrt{T^A_T}} \left[\frac{\gamma}{R} \left(\frac{2}{\gamma + 1} \right)^{\frac{\gamma+1}{\gamma-1}} \right]^{\frac{1}{2}} \tag{3a}$$

where

$$P^A_T = \frac{2 \sum_{1}^{i=n} [(P_T r)_i - (P_T r)_{i-1}](r_i - r_{i-1})}{r^2_{inlet}} \tag{3b}$$

$$T^A_T = \frac{2 \sum_{1}^{i=n} [(T_T r)_i - (T_T r)_{i-1}](r_i - r_{i-1})}{r^2_{inlet}} \tag{3c}$$

and γ is based on T^A_T

For the present study, this definition of reference mass flow was used for both choked and unchoked nozzle flows.

3.1.2 Stream Tube Method

The stream tube discharge coefficient is defined as

$$C_{DS} = \frac{W_a}{W^s_{1\text{-}D}} \tag{4}$$

The reference mass flow ($W^S{}_{1-D}$) is based on sonic flow and a mass flow computed from a finite number of annular stream tube elements of equal area:

$$W^s_{1\text{-}D} = \frac{A^*}{n} \sum_{1}^{i=n} \frac{P_{T_i}}{\sqrt{T_{T_i}}} \left[\frac{\gamma_i}{R} \left(\frac{2}{\gamma_i + 1} \right)^{\frac{\gamma_i+1}{\gamma_i-1}} \right]^{\frac{1}{2}} \tag{5}$$

where γ_i is based on T_{T_i} of each stream tube. Ten stream tube elements were used in the present calculations. This reference mass flow was used for both choked and unchoked nozzle flows.

3.2 THRUST COEFFICIENT

3.2.1 Area-Weighted Method

The area-weighted thrust coefficient is defined as

$$C_{FA} = \frac{F_a}{F^A_{ideal}} \tag{6}$$

The ideal thrust is based on area-weighted stagnation pressure and temperature (Eqs. (3b) and (3c)) outside the wall boundary layer:

$$F^A_{ideal} = W_a \left\{ \frac{2\gamma}{\gamma - 1} RT^A_T \left[1 - \left(\frac{P_c}{P^A_T} \right)^{\frac{\gamma - 1}{\gamma}} \right] \right\}^{1/2}$$

where γ is based on T^A_T.

3.2.2 Stream Tube Method

The stream tube thrust coefficient is defined as

$$C_{FS} = \frac{F_a}{F^s_{ideal}} \tag{7}$$

where

$$F^s_{ideal} = W_a \sum_{1}^{i=n} \frac{1}{n} \left\{ \frac{2\gamma_i}{\gamma_i - 1} RT_{Ti} \left[1 - \left(\frac{P_c}{P_{Ti}} \right)^{\frac{\gamma_i - 1}{\gamma_i}} \right] \right\}^{1/2} \tag{8}$$

and γ_i is based on T_{Ti}. Again, ten stream tube elements (n) were used in the present computations.

3.3 AIRFLOW CALCULATION

The actual nozzle mass flow (W_a) is determined from the main venturi measurements using the calculation procedures outlined in Ref. 10 and a real gas correction (Ref. 11). Based on the individual accuracies of the flow-measuring system and instrumentation, the airflow control system, and real gas corrections, the accuracy of the nozzle airflow is estimated to be ±1 percent.

3.4 NOZZLE THRUST CALCULATION

The measurement of nozzle axial thrust (F_a) is ideally obtained with a thrust stand consisting of a fixed frame, a movable frame, a load cell, and a calibration system. Large thrust-measuring systems of this type are available in the major engine test cells of the ETF. Unfortunately the R-1A-2 test cell is not equipped with a thrust measurement system and available resources precluded development of such a system. In view of this fact, a computed momentum balance procedure was used to determine nozzle thrust.

The actual nozzle gross thrust (F_a) is obtained from a momentum balance based on measured mass flow, measured radial distribution of inlet stagnation pressure and temperature, wall static pressure distributions, computed skin friction and strut drag, and the assumption that static pressure is constant across the nozzle inlet station or

$$F_a = F_i + \int_{A_i}^{A_e} P(x)dA + \int_{A_i}^{A_e} \tau_w dA_\tau - P_c A_e - \text{Drag Strut} \qquad (9)$$

where

$$F_i = P_i A_i + 2\pi \int_{r_{cb}}^{r_w} \rho u^2 r dr \qquad (10)$$

The nozzle inlet static pressure is determined by using the measured radial distribution of stagnation properties and the value of the mass flow obtained from the metering venturi to implicitly solve the integral form of the continuity equation for static pressure. The value of static pressure obtained in this manner generally agreed within 1 to 2 percent of the value for the static pressure measured with a calibrated cone probe. The C8.1 and C15.1 nozzles, however, had high tailpipe Mach numbers (0.7 to 0.9) that resulted in large radial static pressure gradients. Therefore, no thrust computations were made for the C8.1, and only limited thrust computations were made for the C15.1 nozzle configurations. The drag terms in Eq. (9) include an estimate for wall shear force which was obtained from a boundary-layer computer program (Ref. 12). An indication of the boundary layer characteristics of each test nozzle is presented in Fig. 5. The strut drag for the plug nozzles was obtained using the drag coefficient for a cylinder in cross flow. The drag correction for all of the non-plug nozzles except the C8.1 nozzle was less than 1 percent of the nozzle thrust coefficient (C_F). The plug nozzles had a combined calculated strut and wall drag of approximately 1 percent of C_F for the UPAC nozzle and 2 percent of C_F for the SPAC nozzle.

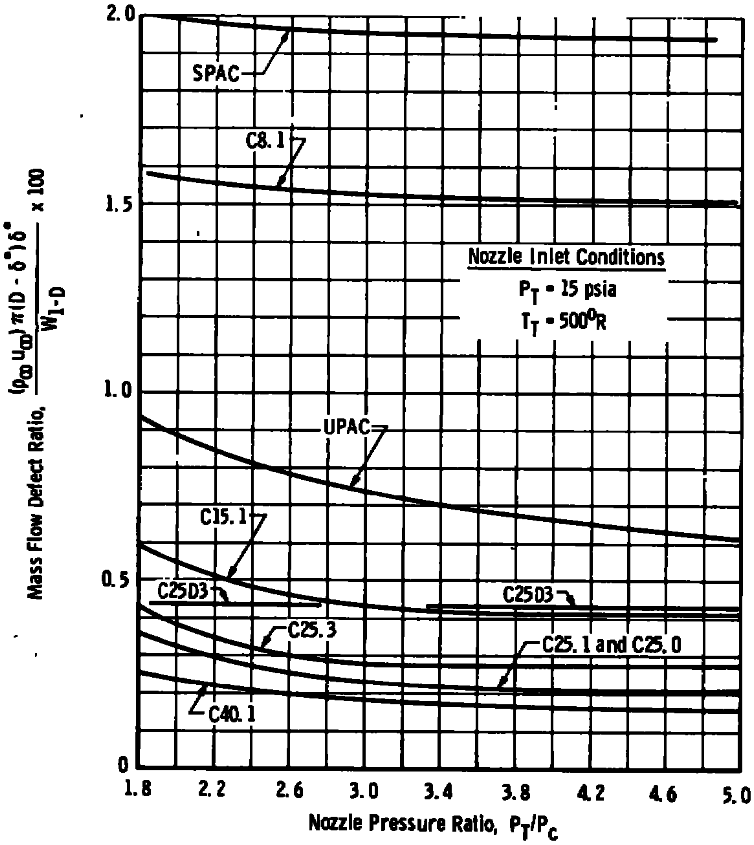

Figure 5. Calculated boundary layer mass defect variation.

The evaluation of nozzle thrust using a computed momentum balance is mechanically simple; however, the accuracy of the thrust is dependent on the individual accuracies of the measured mass flow, the inlet stagnation properties, the wall static pressures, and the calculated wall shear forces. The best estimate of the nozzle thrust accuracy is ±1.5 percent.

4.0 RESULTS

Each nozzle was evaluated in both the turbofan engine exhaust simulator (Fig. 4a) and the uniform flow test rig (Fig. 4b). The general test matrix is presented in the following table[1].

Table 2. Range of Test Conditions

Test Rig	NPR	BPR	BTR	P_T, psia	T_T, °R
Turbofan Simulator	1.8 to 6.0	0.6 to 1.5	0.45 to 1.5	Core: 10 to 20 Secondary: 10 to 20	Core: 500 to 1100 Secondary: 500 to 700
Uniform Flow	1.8 to 6.0	0	1.0	10 to 20	460 to 500

A summary of the data is presented in Appendix A (Nominal Nozzle Performance Data). Theoretical calculations were made with the Wehofer-Moger analysis (Ref. 2) for comparison with experimental data and are included throughout this section. This method uses the asymptotic solution to the time-dependent conservation flow equations. The fluid is assumed to be inviscid, non-heat conducting, and thermally perfect. The flow field is assumed to be axisymmetric or planar. The analysis includes the treatment of both convergent and plug nozzles, and nonuniform nozzle inlet profiles of total pressure, total temperature, and gas properties. Because of the number of calculations required to construct a performance coefficient curve and because of the

[1]It should be noted that, because of the fixed geometry of the turbofan simulator test rig, changes in BPR correspond to changes in the core-to-bypass total pressure ratio. Many turbofan engines have variable geometry features which maintain matched tailpipe stagnation pressure with excursions in BPR. Therefore, the reader should be careful when inferring BPR effects on engine performance from the experimental results presented in this report.

computer time required to construct a flow field for a convergent nozzle including real gas effects, nonuniform inlet flow properties and a free pressure boundary, it was necessary to restrict the theoretical computations to a limited number of test conditions.

4.1 UNIFORM INLET FLOW

4.1.1 Comparison with Other Results

Performance characteristics are compared with Mourey (Ref. 4) to provide a bench mark between the present experiments and previously reported results. Mourey evaluated a 25-deg, convergent, sharp lip nozzle in a cold flow test rig which employed an ASME nozzle for airflow measurement and a static thrust stand equipped with a strain-gage load cell for thrust determination. Experimental discharge coefficients from Mourey and from the present C25.0 nozzle experiments (Fig. 6) agree within 0.75 percent, with the maximum

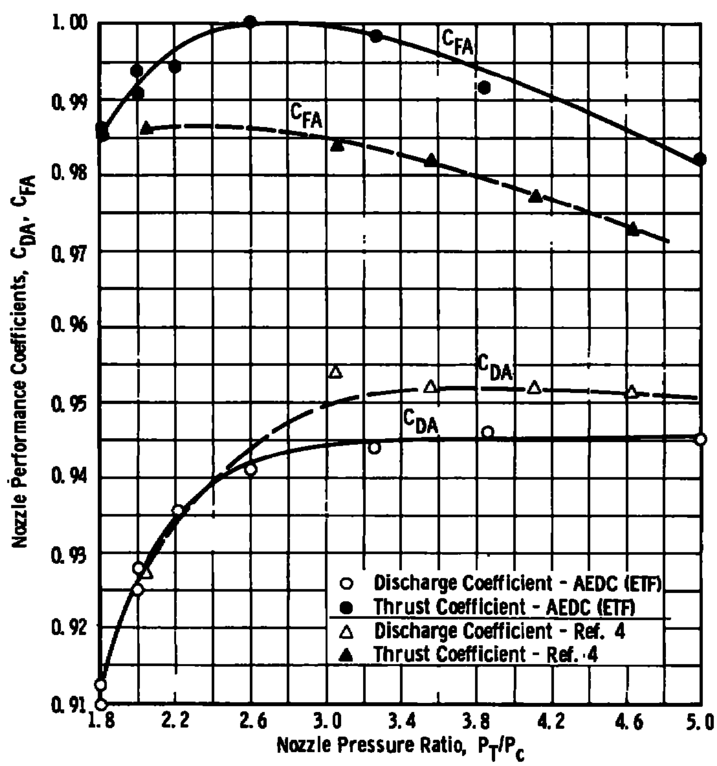

Figure 6. Comparison of C25.0 nozzle performance from different test rigs (uniform cold flow inlet conditions).

deviation occurring at nozzle pressure ratios above 3. Thrust coefficients agree to within 1 to 1.5 percent, which is reasonable in view of slight differences in contraction ratio and boundary layer characteristics between test configurations.

Previous AEDC investigations (Ref. 2) demonstrated the correlation between theoretical calculations made with the Wehofer-Moger analysis and all the sharp lip conical nozzle data obtained by Mourey (Fig. 7). Also shown in Fig. 7 is a comparison of the present C25.0 nozzle performance results. There is good agreement between the calculated discharge coefficients and all the experimental results. Differences between the theoretical thrust coefficients and the experimental results are somewhat greater, possibly because of the larger uncertainty in measured thrust as compared with measured mass flow.

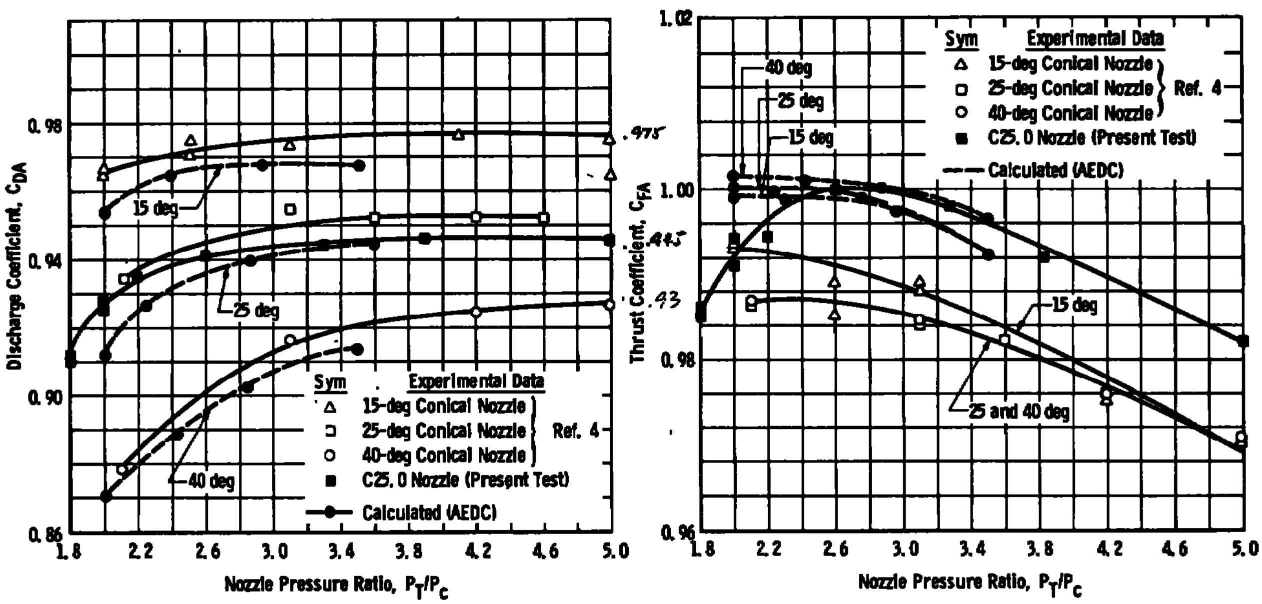

a. Discharge coefficient

b. Thrust coefficient

Figure 7. Comparison of experimental and theoretical convergent conical nozzle performance (uniform cold flow).

A comparison of nozzle performance coefficients for the two plug nozzles (UPAC and SPAC) and similar nozzles reported by Glasgow (Ref. 5) is presented in Figs. 8a and b. Glasgow used a choked venturi to measure mass flow and a force balance system for thrust measurements. Because the SPAC nozzle throat is located upstream of the nozzle exit and there is a significant region of supersonic flow which isolates the throat from ambient pressure, the discharge coefficient is nearly constant with pressure ratio. The data comparison shows a maximum 0.75-percent difference in discharge coefficients and a difference of approximately 2 percent in thrust coefficients. The uncertainty in thrust coefficients from the present studies is expected to be largest for the plug configurations since these nozzles have the fewest wall pressure taps and largest correction for wall shear and strut form drag. There is generally good agreement between the experimental and theoretical wall pressure distributions for the UPAC nozzle (Fig. 9). The difference in the aft end plug pressure distribution for X greater than 1.6 is attributed to the presence of a shock or flow separation. The present theoretical procedure does not account for either flow phenomenon. Comparison of theoretical and experimental discharge and thrust coefficients for the UPAC nozzle is included in the table in Fig. 9.

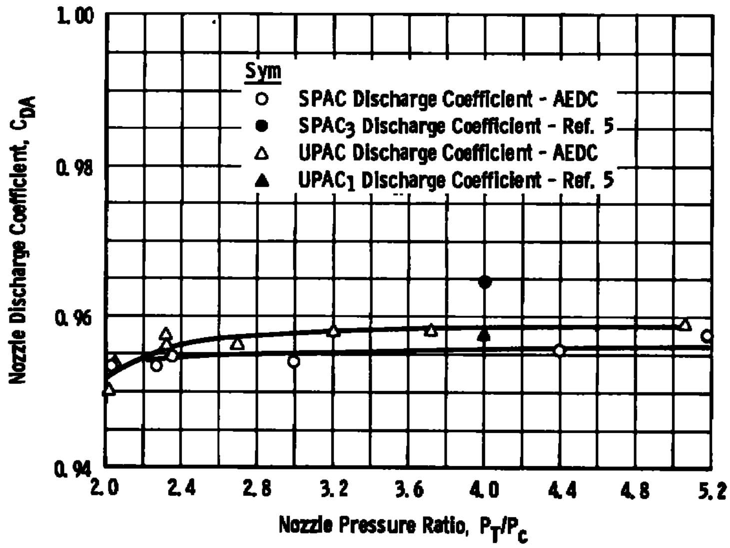

a. Discharge coefficient

Figure 8. Comparison of plug nozzle performance from different test rigs (uniform cold flow inlet conditions).

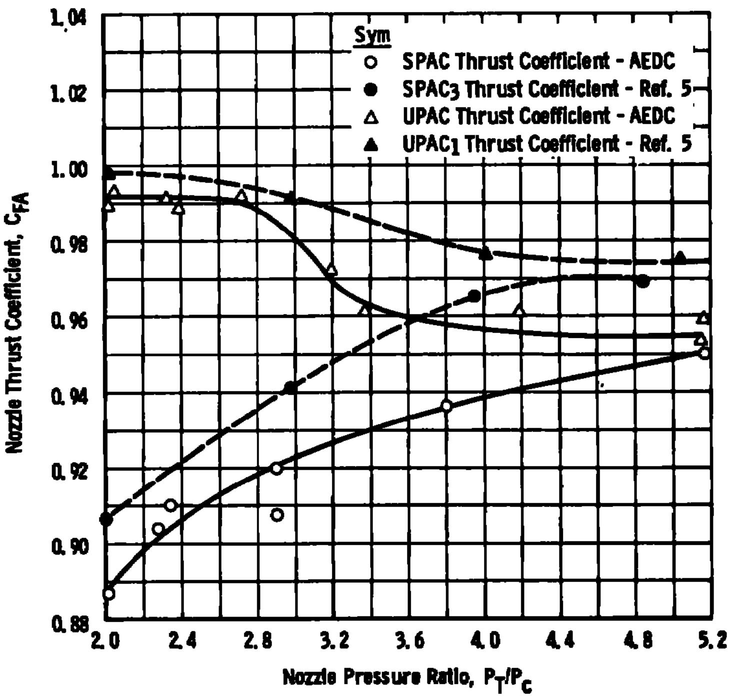

b. Thrust coefficient
Figure 8. Concluded.

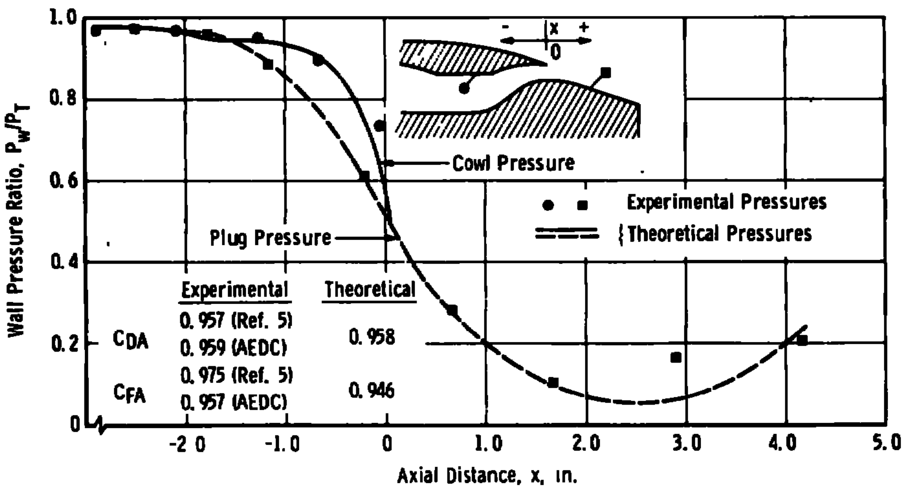

Figure 9. Unshrouded plug nozzle pressure distribution (cold flow, NPR = 4.0).

In summary, within the limits of uncertainty imposed by

1. slight differences in geometry,
2. some differences in inlet flow conditions, particularly boundary layer characteristics, and
3. accuracy of the measuring system involved,

the current experimental results are in general agreement with those of Mourey and Glasgow. Also, for uniform nozzle inlet flow, there is generally good agreement between the theoretical calculations and the experimental data.

4.1.2 Nozzle Throat Geometry Effects

The influence of changes in throat geometry on nozzle wall Mach number distribution can be evaluated by comparing distributions for a sharp-lip convergent nozzle (C15.0 and C25.0) and one having a rounded lip (C15.1 and C25.1) (Fig. 10). A rounded lip causes the flow to rapidly accelerate in the vicinity of the throat region when compared with a sharp-lip nozzle. A comparison of a theoretical (Ref. 2) wall pressure distribution with experimental data is shown in Fig. 11. As evidenced by the experimental results, the flow separates from the nozzle wall in the vicinity of the nozzle throat. For nozzles having a small throat radius of curvature (~0.1), the flow can apparently withstand approximately 10-percent rise in back pressure before separating (Figs. 12a and b). This 10-percent criterion can be used in making nozzle flow calculations. For larger throat radius of curvatures (~0.3), the rise in back pressure does not result in the abrupt change in wall pressure (Fig. 12c). For the larger throat radii of curvature, additional information (i.e., throat wall pressures) is required before calculations can be made for an overexpanded flow field.

Although the flow does apparently separate, the rounded lip still exerts an influence on the outer portion of the nozzle flow field. The influence of throat geometry on nozzle performance characteristics can be determined from a comparison of the experimental results from the C25.0, C25.1, C25.3, and C25D3 nozzles. Increasing nozzle lip radius of curvature increased both discharge and thrust coefficients (Fig. 13). A comparison of theoretical and experimental performance coefficients is illustrated in Fig. 14. In making the theoretical calculations for the C25.3 nozzle, the point of flow separation was estimated from the experimental wall pressures. The analytical and experimental discharge coefficients are in relatively good agreement. The analytical results, however, did not predict the experimentally observed difference in thrust coefficient between the C25.3 and the C25.0 nozzles. Nor did the theoretical calculations predict the drop-off of the thrust coefficient for the C25.0 and C25.3 nozzles at the lower pressure ratios. However, the difference in the theoretical and experimental thrust coefficients is within the expected accuracy of the momentum balance procedure. A more accurate thrust measurement is apparently required to resolve this particular thrust anomaly between the experimental and theoretical results.

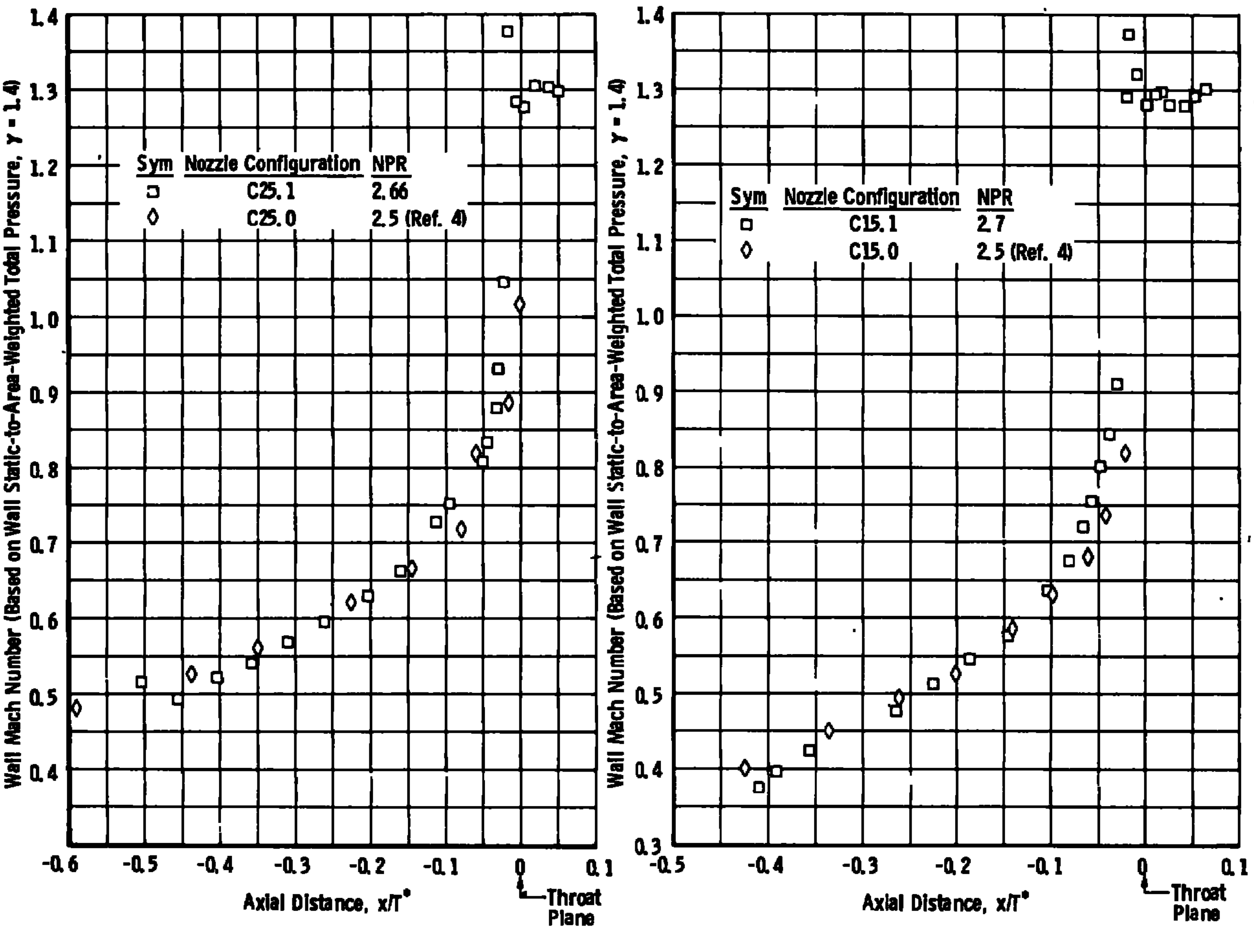

a. 15-deg conical nozzle

b. 25-deg conical nozzle

Figure 10. Influence of nozzle throat geometry on wall Mach number distribution.

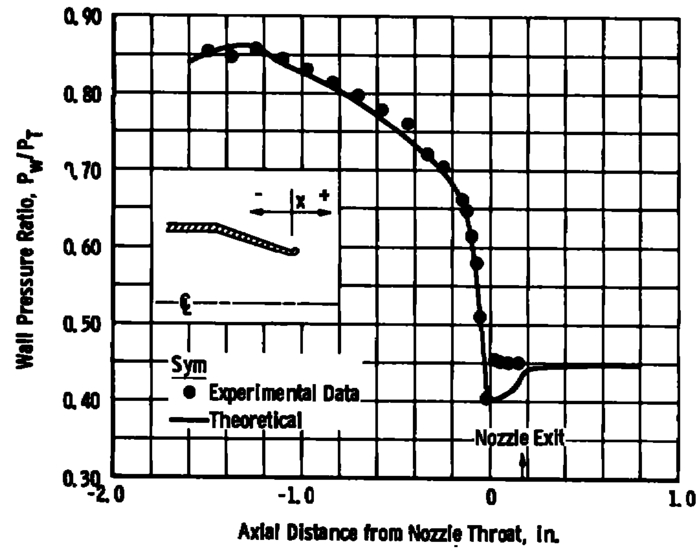

Figure 11. Comparison of theoretical and experimental C15.1 nozzle wall pressure distributions (cold uniform flow, NPR = 2.22).

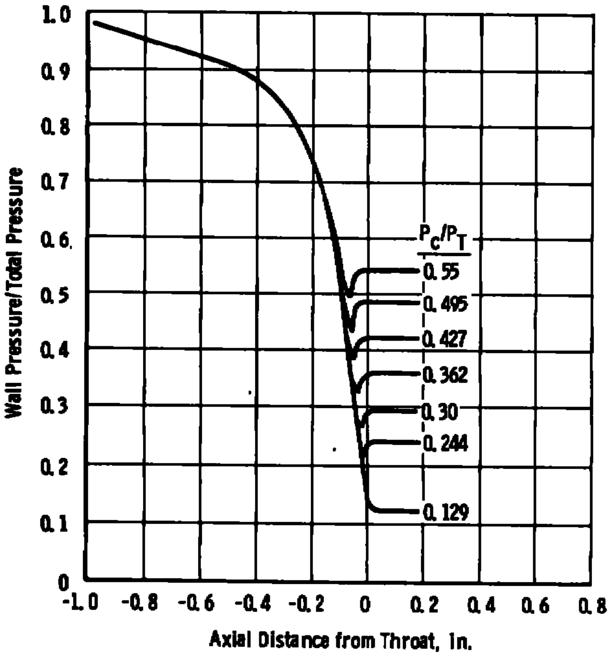

a. C40.1 nozzle

Figure 12. Influence of exhaust pressure on wall pressure distribution (from cold flow experiments).

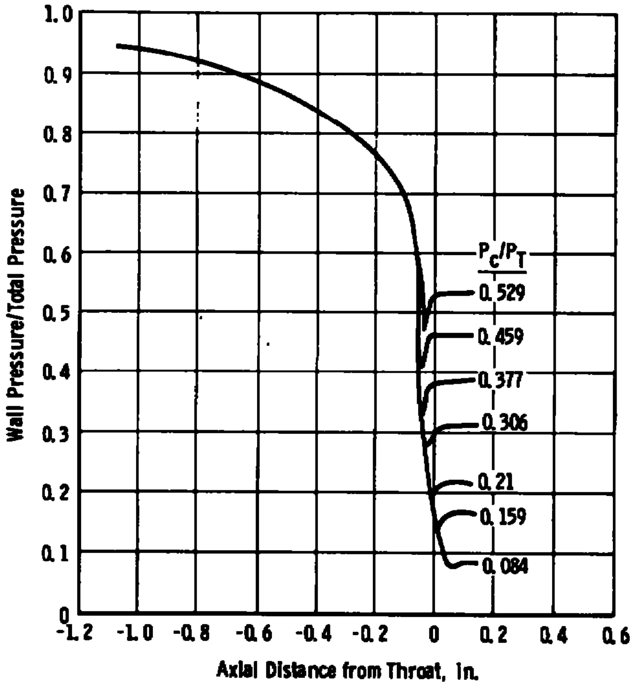

b. C25.1 nozzle

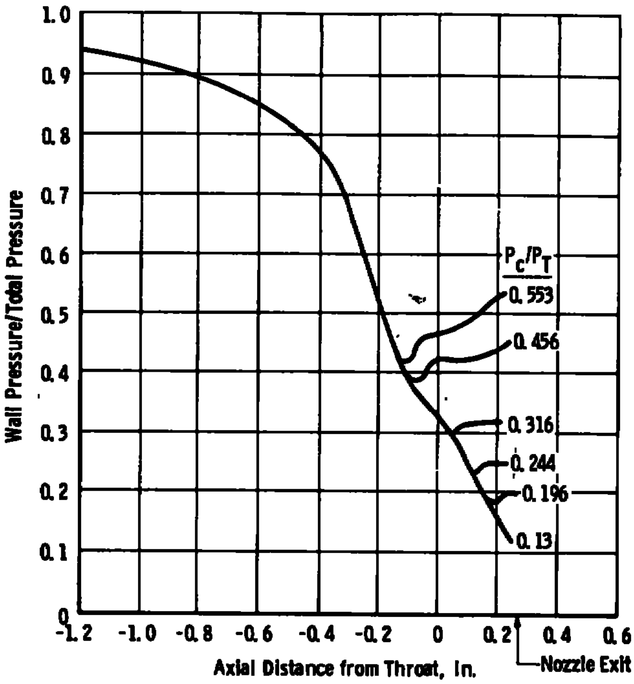

c. C25.3 nozzle
Figure 12. Concluded.

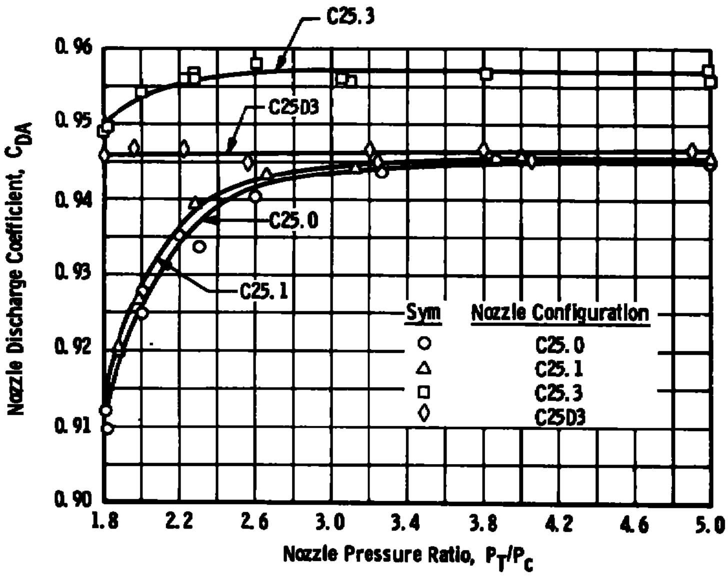

a. Discharge coefficient

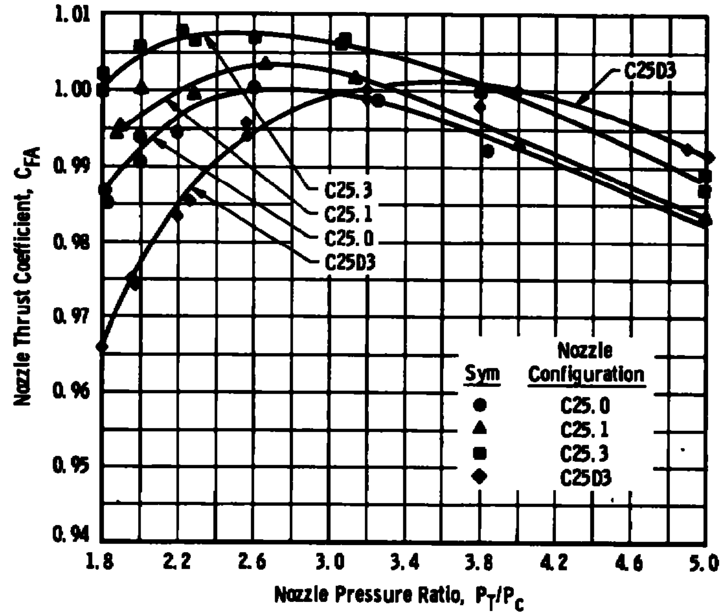

b. Thrust coefficient

Figure 13. Influence of nozzle throat geometry on nozzle performance (uniform cold flow).

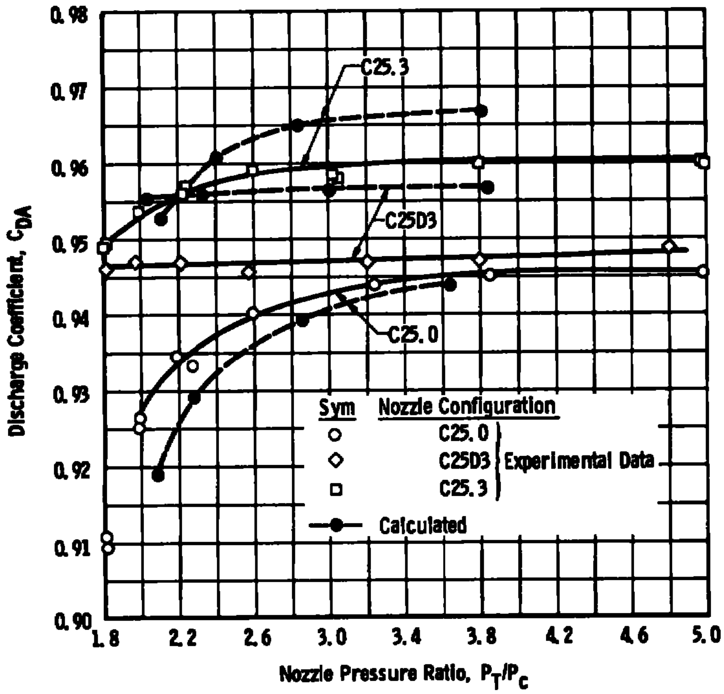

a. Discharge coefficient

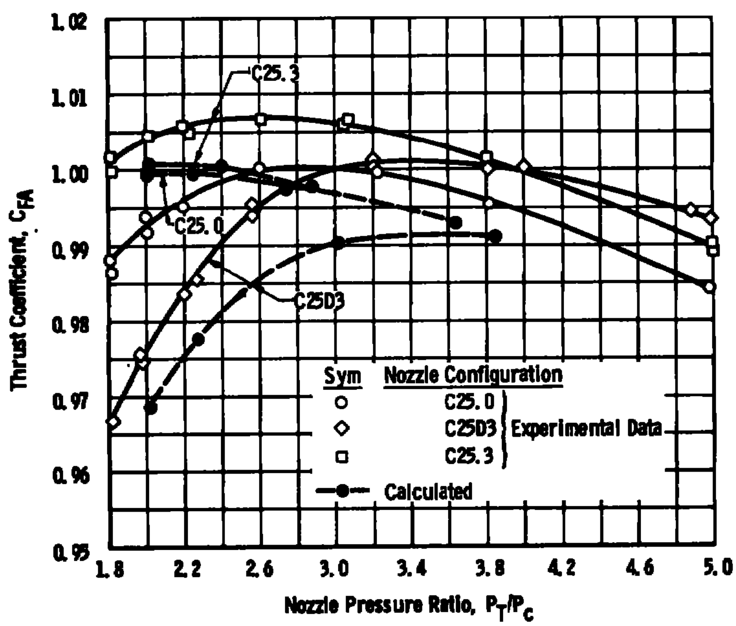

b. Thrust coefficient

Figure 14. Comparison of experiment and theory for 25-deg convergent nozzles.

4.2 EFFECT OF TOTAL PRESSURE DISTORTION (COLD PRIMARY FLOW)

The influence of radial distortions in total pressure on nozzle performance was evaluated in the turbofan simulator test rig (Fig. 4b). Unheated air was used for both the primary and bypass streams. The nozzle inlet radial total pressure profiles were obtained by altering the inlet total pressure to the bypass and main venturis.

Typical nozzle total pressure profiles obtained with the C40.1 nozzle are presented in Fig. 15 for bypass ratios of 0.81 and 1.36. For a BPR of 0.81, the total pressure of the core flow is greater than that of the bypass flow. Increasing the BPR to 1.36 results in a bypass total pressure greater than that of the core flow. Also, for comparative purposes, typical total pressure profiles for a full-scale turbofan with BPR ~ 1 and for a turbojet engine operating at military power conditions are presented in Fig. 15. The nozzle wall pressure data did not reveal any distinguishing characteristic of inlet pressure distortion on wall pressure distribution. However, a consistent effect of inlet pressure distortion on nozzle discharge coefficient was observed (Figs. 16 and 17). As the BPR increases (i.e., increasing bypass total pressure), the nozzle discharge coefficient decreases. This trend was observed for all the nozzles over the entire range of flow conditions investigated. For nozzle pressure ratios greater than approximately 2.6, there is no appreciable difference in nozzle thrust coefficients from uniform and nonuniform inlet pressure profiles. There are, however, some discernible differences in uniform and nonuniform flow thrust coefficients at the lower nozzle operating pressure ratios. It basically appears that pressure distortions have a more pronounced effect on discharge coefficient than on nozzle thrust coefficient. Although not shown, there are essentially no differences between the thrust or discharge coefficients obtained using the area-weighted or the stream tube referencing methods.

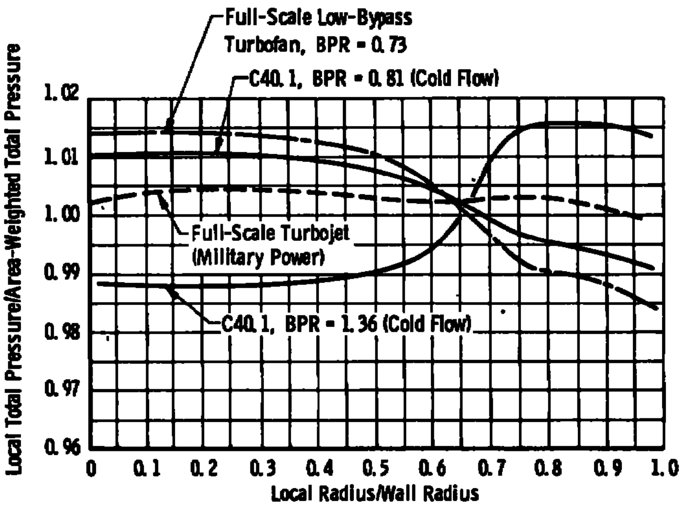

Figure 15. Radial distribution of total pressure at nozzle inlet plane.

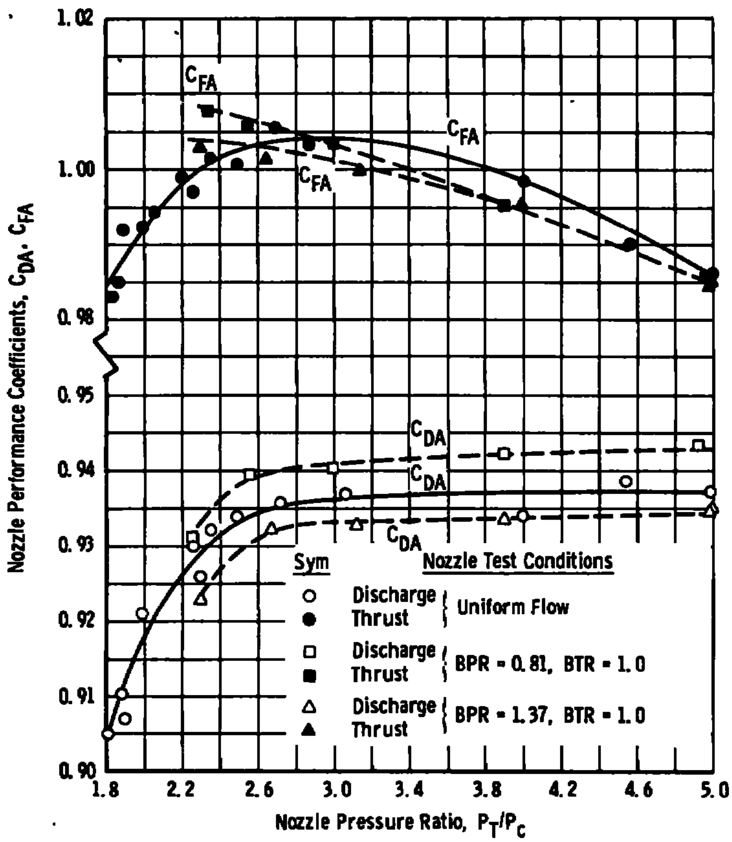

Figure 16. Influence of nozzle bypass ratio on C40.1 nozzle performance (cold flow).

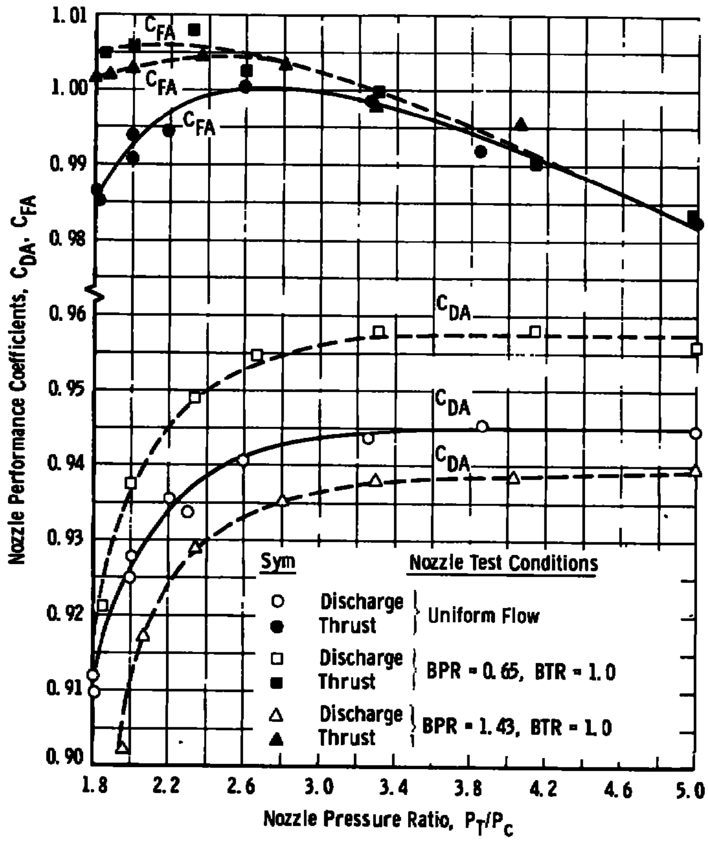

Figure 17. Influence of nozzle bypass ratio on C25.0 nozzle performance (cold flow).

4.3 EFFECT OF COMBINED TOTAL PRESSURE AND TEMPERATURE DISTORTION

The influence of the combined radial distortion of both total pressure and temperature on nozzle performance was also evaluated in the turbofan simulator test rig (Fig. 4a). Heated air (800 to 1100°R) was used for the primary airstream and unheated air (500°R) was used for the bypass flow. Again, the nozzle inlet radial profiles were varied by altering the inlet total pressure to the bypass and main venturis. Typical nozzle total temperature profiles for the present investigations and profiles for a full-scale turbofan and turbojet at military power conditions are shown in Fig. 18. Temperature distributions in the present experiments closely approximate the full-scale low-bypass turbofan conditions.

Typical nozzle total pressure and temperature profiles obtained with the C25.0 nozzle are presented in Fig. 19 for BPR's of 1.37 and 0.785 and BTR's of 0.515 and 0.65, respectively. Additional pressure and temperature profiles for each nozzle are presented in Appendix B (Nozzle Pressure and Temperature Profiles).

For Mi ~0.4 (see page 11)

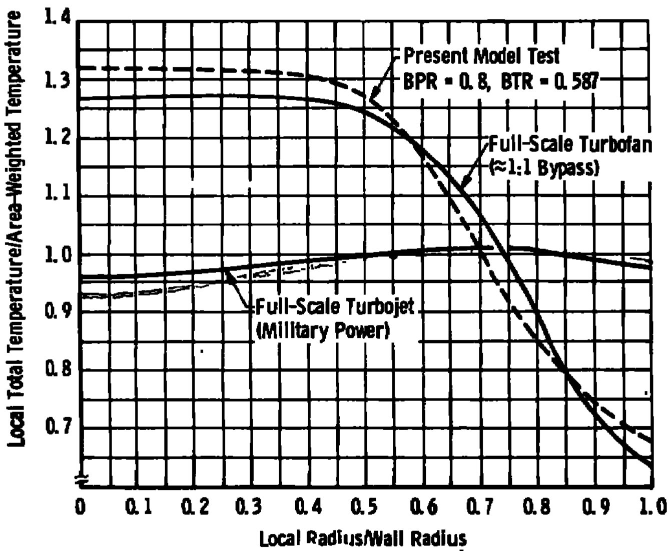

$\frac{V}{V_\infty}$

$\frac{.93-1}{.93} = -.08$

Figure 18. Comparison of radial total temperature profiles at nozzle inlet.

$\frac{1.4}{.6} = 2.35$

$\frac{1.41-.6}{1.41} = 0.574$

$\frac{1.18}{.85} = 1.38$

$\frac{V}{V_\infty}$ $\frac{1.18-.85}{1.18} = 0.28$

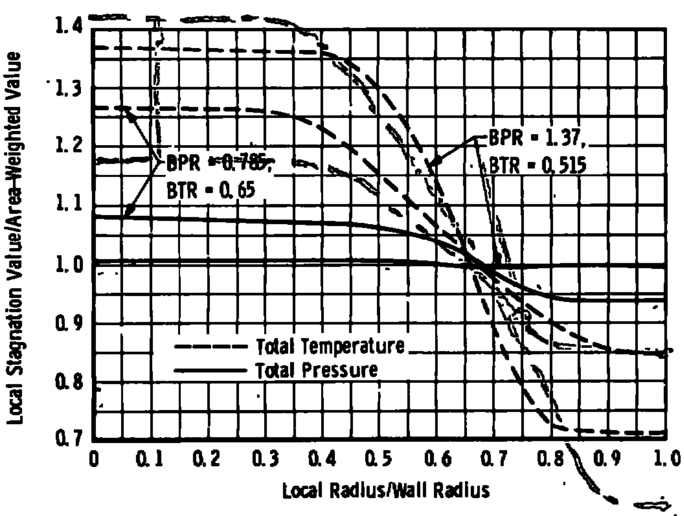

Figure 19. Inlet stagnation properties for C25.0 nozzle at two nonuniform inlet temperature conditions.

Once again, there are no distinguishing characteristics of nozzle inlet pressure-temperature distortions as compared with undistorted flow on wall Mach number distributions (Fig. 20). Nozzle C25.0 performance coefficients obtained with inlet temperature and pressure distortions are compared in Figs. 21 and 22 with uniform flow and with distorted pressure results. Whereas changes in pressure distortion principally affect discharge coefficient, changes in bypass temperature ratio influences both the area-weighted discharge and thrust coefficients. As shown in Section 4.2, increasing the BPR decreased the discharge coefficient. However, Fig. 22 shows that the discharge coefficient increased for an increase in BPR. Therefore, the effect on the area-weighted discharge coefficient of the temperature distortions is opposite to the effect of the pressure distortions. Also, whereas pressure distortions alone had what is considered to be a secondary effect on the area-weighted thrust coefficient, the presence of both pressure and temperature distortions resulted in a significant shift in magnitude but not in shape of the area-weighted thrust coefficient curve (Fig. 22).

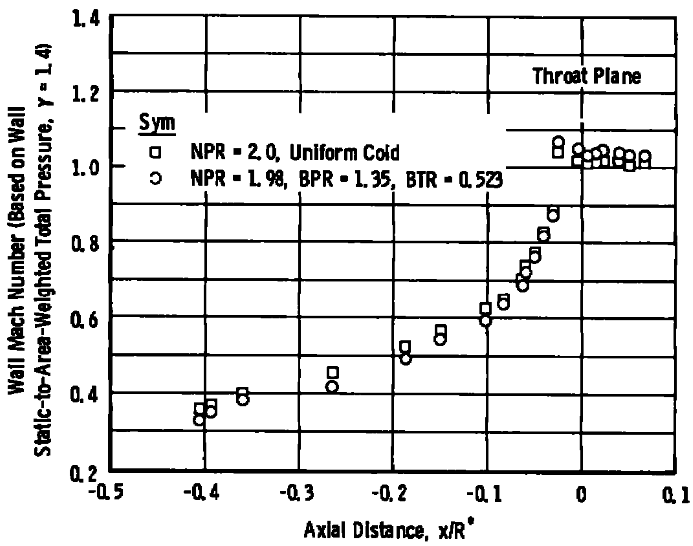

a. Nozzle pressure ratio ~ 2.0

Figure 20. Wall Mach number distribution for various nozzle inlet temperature profiles (C25.1 nozzle).

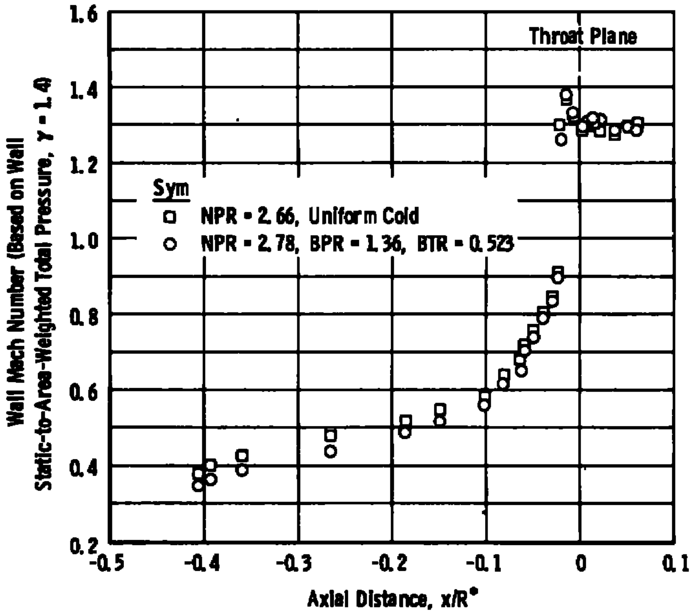

b. Nozzle pressure ratio ~ 2.7

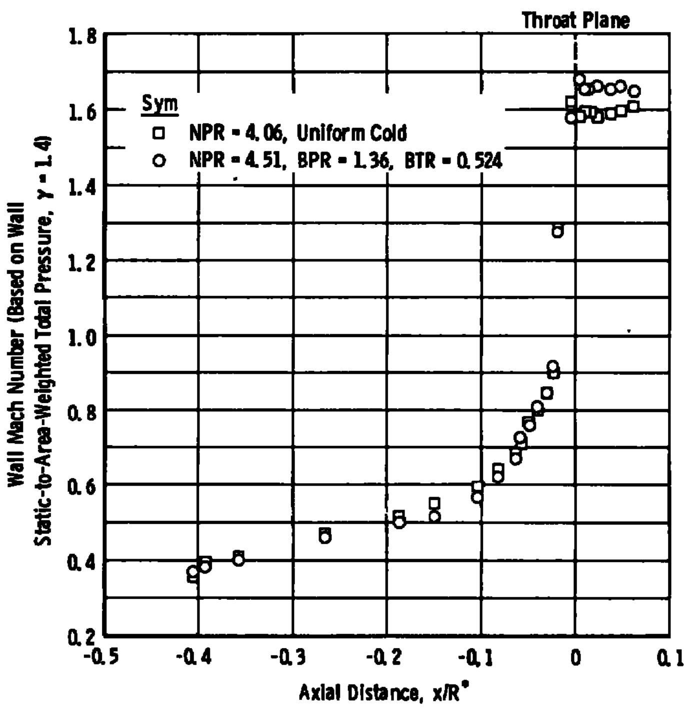

c. Nozzle pressure ratio ~ 4.3

Figure 20. Concluded.

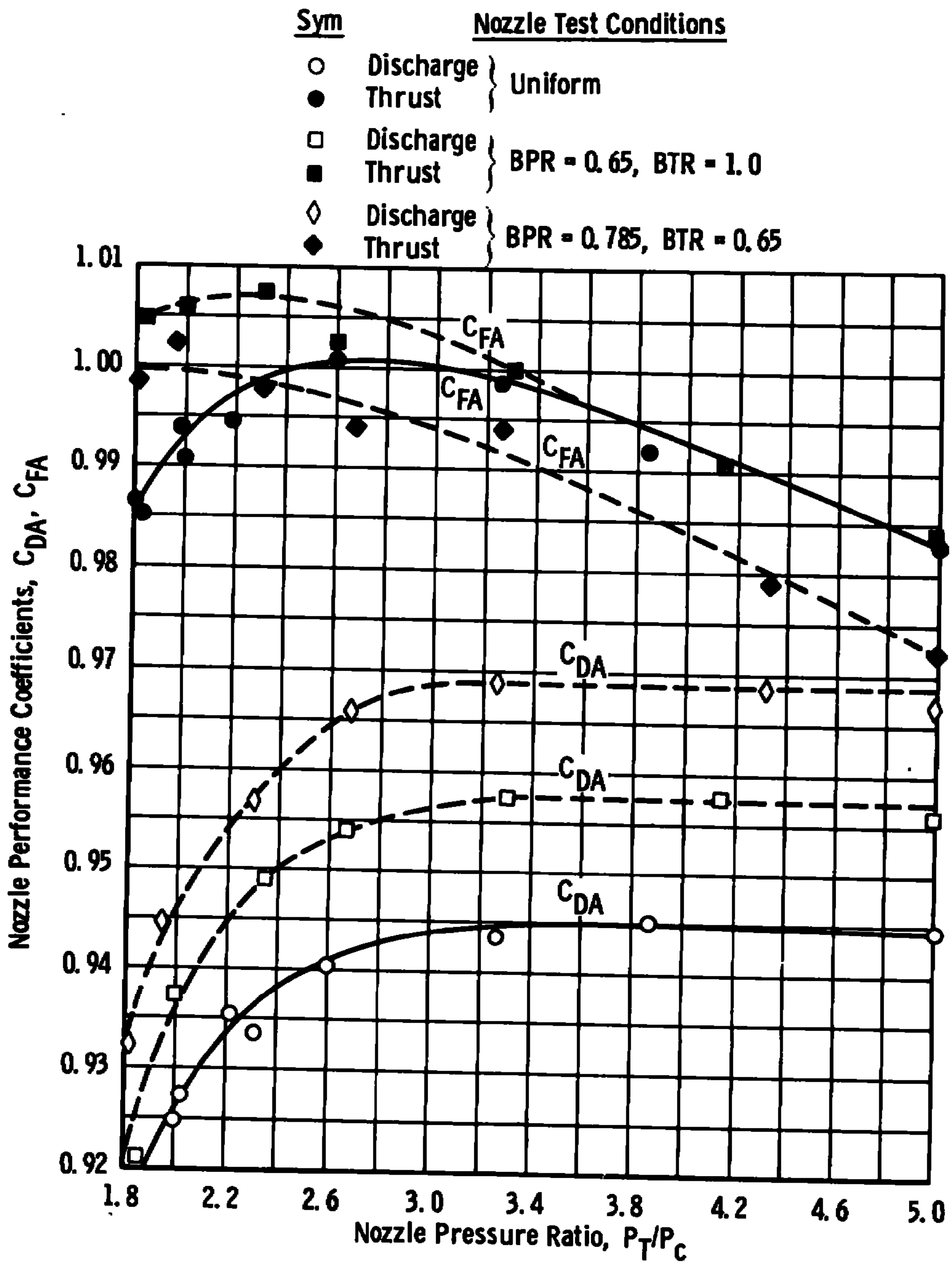

Figure 21. Influence of nozzle bypass ratio on C25.0 nozzle performance (cold versus hot core flow).

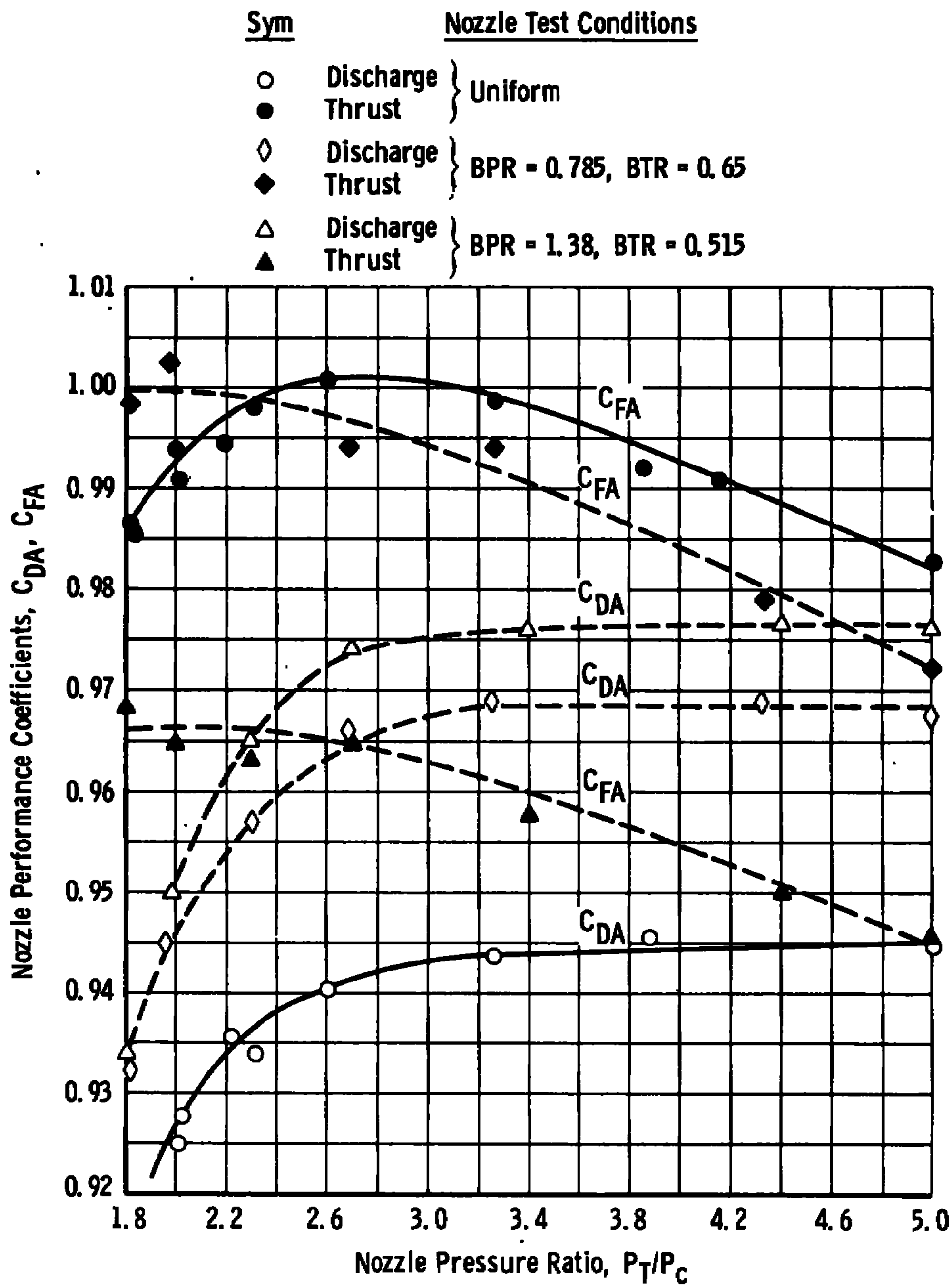

Figure 22. Influence of nozzle bypass ratio on C25.0 nozzle performance (hot core flow versus uniform flow).

A comparison of theoretical and experimental results for the C25.1 nozzle is presented in Fig. 23. Experimentally measured inlet stagnation conditions were used as inputs for the theoretical calculations. While the theoretical results compare favorably with the experimental data, the theoretical results for nonuniform flow are not as consistent as the uniform flow results as evidenced by the discontinuity of the line interconnecting the theoretical points (Fig. 23). The discontinuity in the theoretical results for the nonuniform flow is principally the result of having large radial gradients in the stagnation flow properties. Because of these gradients, the nonuniform theoretical results are not as stable numerically as the uniform results. The numerical instabilities require that additional analytical restraints be applied to the finite differencing scheme (Ref. 2). Several hours of IBM 370/155 computer time were required to obtain the nine theoretical calculations presented in Fig. 23. This relatively large amount of computer time is required to establish the boundaries of the free-jet flow field for conical nozzles. This is necessary since the flow field at the exit plane of conical convergent nozzles is not entirely choked (Ref. 1), and therefore, the free-jet flow field influences the internal nozzle performance. Also, when there are radial gradients of stagnation pressure and temperature, it is necessary to use as fine a grid mesh network as possible in order to obtain accurate results.

Additional comparisons of theoretical and experimental results are presented in Fig. 24, where wall pressure distributions for the C25D3 nozzle are shown. The difference in the theoretical and experimental pressure distribution just downstream of the nozzle throat is assumed to be the result of a local separation bubble. Since the divergent portion of this nozzle is physically defined, the C25D3 nozzle calculations require much less computer time than the conical nozzle calculations. The analytical results presented in Fig. 25 were obtained with a 21 by 56 mesh incorporating real gas effects in about 30 min of IBM 370/155 computer time. The influence of flow nonuniformities on discharge coefficients (Fig. 25) for plug nozzles is similar to that of non-plug nozzles; decreasing the bypass temperature ratio increases the discharge coefficient. Unlike the non-plug nozzles, the nonuniformities increased the plug nozzle area-weighted thrust coefficients relative to the uniform flow results.

The nozzle performance coefficients presented in Figs. 13 to 25 used the area-weighted stagnation properties in the definition of reference conditions. A comparison between area-weighted and stream tube performance coefficients for the C25.1 nozzle is presented in Fig. 26. Using the stream tube referencing procedure as compared with the area-weighted method generally brings the nozzle coefficients more in line with the uniform flow results. However, coefficients obtained with either referencing procedure can deviate considerably from uniform flow results when significant distortion in inlet stagnation properties exists.

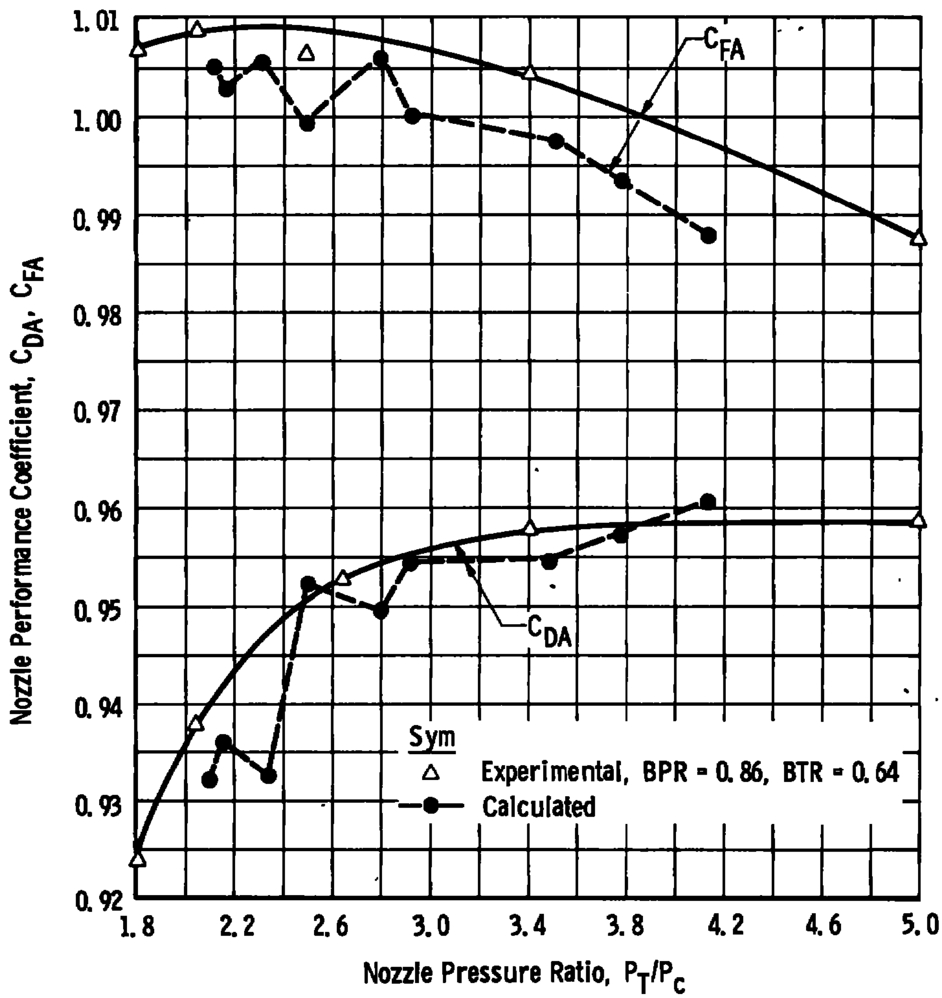

Figure 23. Comparison of experimental and theoretical nonuniform C25.1 nozzle performance.

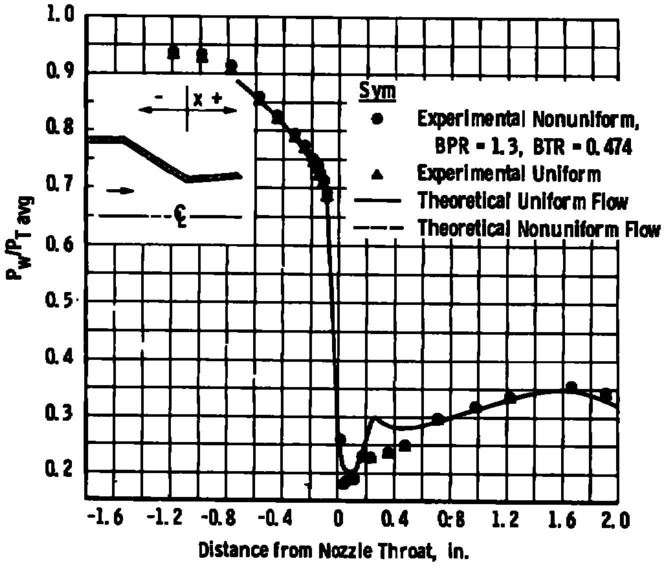

Figure 24. Comparison of theoretical and experimental wall pressure distribution for convergent-divergent (C25D3) nozzle (NPR = 3.0).

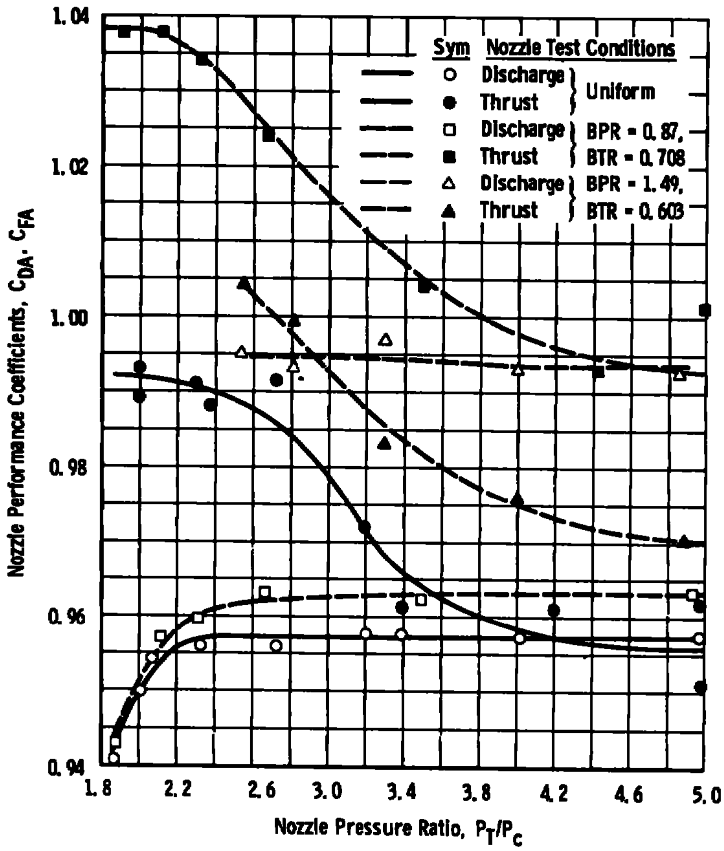

Figure 25. Influence of nozzle bypass ratio on UPAC nozzle performance (hot core flow versus uniform flow).

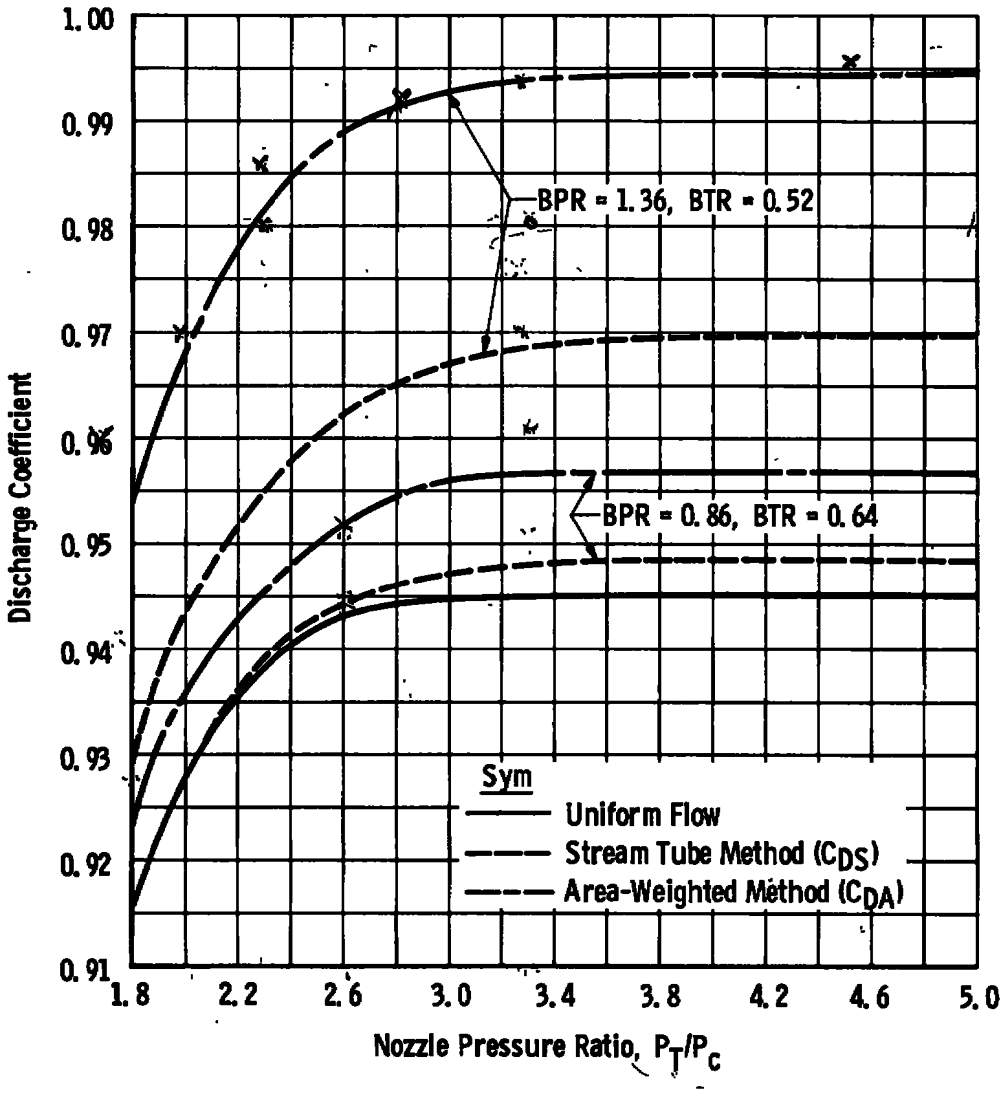

a. Discharge coefficient
Figure 26. Influence of referencing condition on nozzle performance coefficient (C25.1 nozzle).

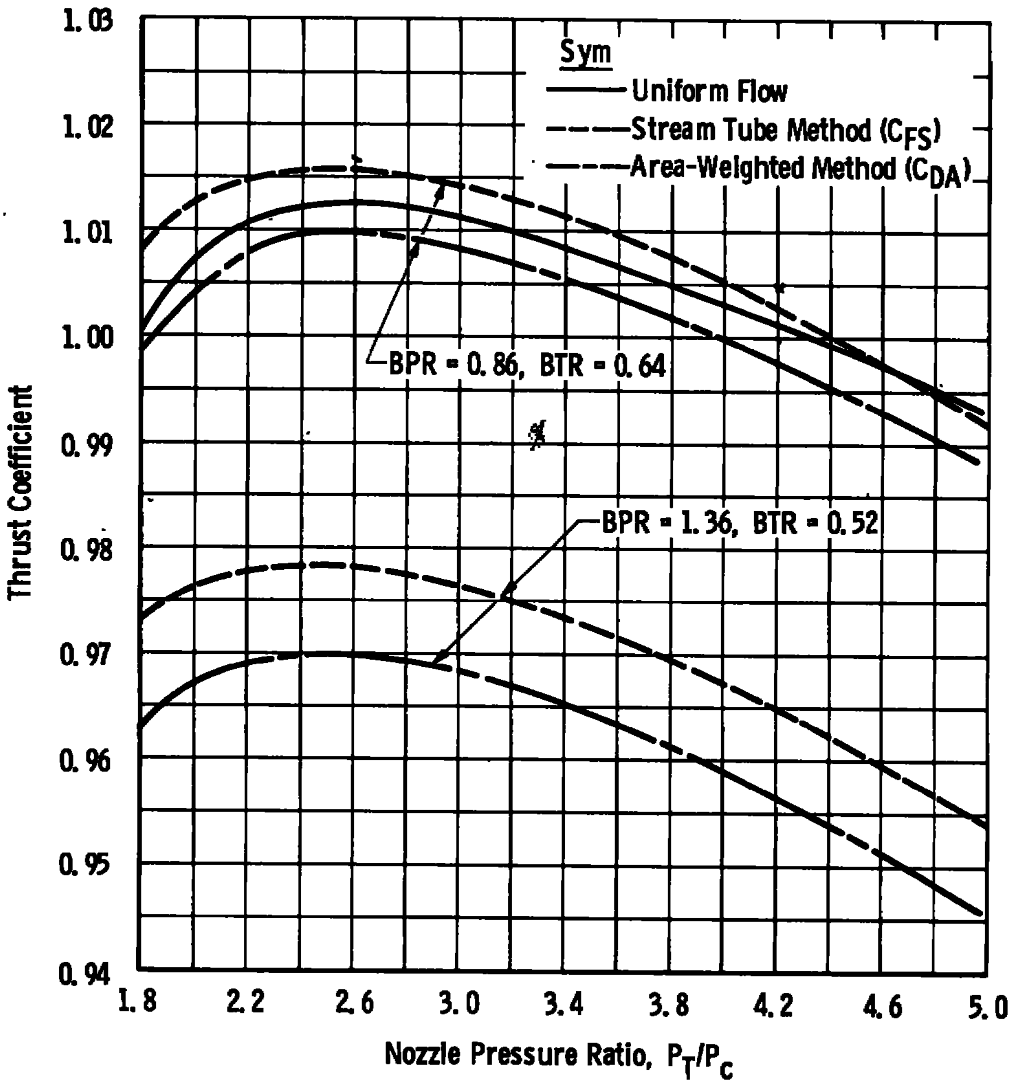

b. Thrust coefficient
Figure 26. Concluded.

5.0 SUMMARY

The primary objective of the turbine engine exhaust nozzle investigations was to experimentally determine and analytically verify the influence of nozzle inlet flow nonuniformities and geometry effects on nozzle performance characteristics. Critical-flow venturis were used to measure nozzle mass flows to an estimated accuracy of ±1 percent. Nozzle thrust was evaluated using a momentum balance procedure to an estimated accuracy of ±1.5 percent.

The present experimental results for undistorted nozzle flows were generally in good agreement with the experimental results of other investigators. For plug nozzles, the experimental thrust values deviated approximately 2 percent from the experimental values presented by Glasgow. The thrust uncertainty for the present tests are expected to be largest for the plug nozzles. The theoretical calculations for undistorted inlet flow for non-plug and plug nozzles agreed with experimental discharge coefficients to within 1 percent. The agreement between theoretical and experimental thrust coefficients for plug (using present experimental results) and non-plug nozzles was approximately 1.5 percent.

The experimental data show a significant influence of small changes in nozzle throat geometry on discharge coefficient. As expected, increasing the throat radius of curvature increases the discharge coefficient. This result was also verified by the theoretical results. The theoretical and experimental data, however, are in disagreement with respect to the influence of changes in throat radius on thrust coefficient. The experimental data reflect an increase in thrust coefficient with increasing curvature, but the theoretical results indicate virtually no change. Since the difference in thrust coefficient is approximately 1 percent, a more accurate thrust measurement than the present momentum balance is required to resolve this difference.

The present experimental results demonstrated that cold flow pressure distortions representative of low-bypass turbofans have a noticeably more pronounced effect on discharge than on thrust coefficients obtained from either the area-weighted or the stream tube referencing techniques. Whereas changes in pressure distortion principally affect discharge coefficient, changes in bypass temperature ratio influences both the discharge and thrust coefficient. For nozzle performance coefficients versus nozzle pressure ratio, the effect of pressure and temperature distortion results in a shift in magnitude but generally not a significant change in the shape of the curves.

The present experimental data indicate that nozzle wall pressure and Mach number distributions have very limited value for predicting or analyzing the effects of distortion on nozzle performance.

When making theoretical calculations for distorted nozzle flows, the numerical results would exhibit instabilities in flow properties in the vicinity of large gradients in stagnation properties. However, by using the additional analytical restraints discussed in Ref. 2, these numerical instabilities were eliminated and generally good correlation (±1.5 percent) with the experimental results was maintained. The Wehofer-Moger computer program requires relatively substantial computer time and operational experience, particularly for free-jet calculations; however, the program has demonstrated it can provide predictions for rather complex nozzle flows.

Using the stream tube referencing procedure compared with the area-weighted method generally brings the nozzle coefficients more in line with the uniform flow results. However, depending on the type of flow distortions, either referencing procedure can deviate considerably from uniform flow results. Therefore, it can be concluded that nozzle performance coefficients cannot be ascribed to a given nozzle configuration without regard for nozzle inlet flow conditions. This conclusion is also confirmed by the theoretical results.

REFERENCES

1. Wehofer, S. and Moger, W. C. "Transonic Flow in Conical Convergent and Convergent-Divergent Nozzles with Non-uniform Inlet Conditions." AIAA 6th Propulsion Joint Specialists' Conference, Paper No. 70-635, June 15-19, 1970.

2. Wehofer, S. and Moger, W. C. "Analysis and Computer Program for Evaluation of Airbreathing Propulsion Exhaust Nozzle Performance." AEDC-TR-73-29 (AD760541), May 1973.

3. Grey, R. E. and Wilsted, H. D. "Performance of Conical Jet Nozzles in Terms of Flow and Velocity Coefficients." NASA Report 933, 1949.

4. Mourey, W. L. "Test Data Report - Flow Characteristics Including Sonic Line Determination for Four Convergent Nozzles." Boeing Company Report T6-5478-1, Vol. I, April 1968.

5. Glasgow, E. R., et al. "Experimental and Analytical Determination of Integrated Airframe Nozzle Performance." AFFDL-TR-72-101, Vols. I and II, October 1972.

6. Mikkelson, D. C. and Head, V. L. "Flight Investigation of Airframe Installation Effects on a Variable Flap Ejector Nozzle of an Underwing Engine Nacelle at Mach Numbers from 0.5 to 1.3." NASA TMX-2010, 1970.

7. Boytos, J. F. "Gross Thrust Coefficient-Turbofan Engine." Journal of Aircraft, Vol. 6, No. 6, pp. 565, November-December 1969.

8. Hatt, F. G. and Hancock, D. M. "Recent Flight Experience with the F100 Engine in the YF-16." AIAA/SAE 10th Propulsion Conference, Paper No. 74-1163, October 21-23, 1974.

9. Bernstein, A., et al. "Compound-Compressible Nozzle Flow." Journal of Applied Mechanics, Paper No. 67-APM-L, 1956.

10. Smith, R. E., Jr. and Matz, R. J. "A Theoretical Method of Determining Discharge Coefficients for Venturis Operating at Critical Flow Conditions." American Society of Mechanical Engineers, Journal of Basic Engineering, Vol. 84, Series D, No. 4, pp. 434, December 1962. Dec 1962

11. Johnson, R. C. "Real-Gas Effects in Critical Flow through Nozzles and Tabulated Thermodynamic Properties." NASA TN D-2565, January 1965.

12. Weingold, A. O. "The ICRPG Turbulent Boundary-Layer Reference Program." Pratt and Whitney Aircraft, July 1968.

APPENDIX A
NOMINAL EXPERIMENTAL NOZZLE PERFORMANCE DATA

Data Point	P_{T_a}, psia	T_{T_a}, °R	NPR	BPR	C_{DA}	C_{FA}	$\dot{w}_a$, lbm/sec	F_a, lbf	T_{T_p}, °R	T_{T_B}, °R
Nozzle C15.1										
64- 20	11.78	727	6.03	0.75	0.986	0.94	5.337	292	974	533
- 30	11.64	729	2.95		0.983	0.966	5.272	240	977	534
- 40	11.86	733	1.970		0.971	0.966	5.281	198	983	537
- 50	12.14	733	1.76		0.952	0.963	5.275	180	983	536
- 60	12.32	735	1.660		0.934	0.963	5.246	171	986	540
- 70	11.95	737	1.86		0.963	0.9615	5.276	190	988	540
- 80	11.72	735	2.40		0.983	0.967	5.265	220	987	539
- 90	11.79	737	3.89		0.985	0.961	5.287	268	988	540
-100	9.908	493	5.33	1.24	0.947	0.98	5.260	238	*	*
-110	9.962	493	2.54		0.945	1.0	5.258	193		
-120	10.26	493	1.76		0 914	0.995	5.239	150		
-130	10.69	495	1.56		0.877	0 99	5 214	135		
-140	10.73	499	1 48		0.855	0 988	5 175	116		
-150	10.47	500	1.63		0.891	0.99	5 186	139		
-160	9.781	503	2.07		0 937	1.0	5.171	165		
-170	9.886	504	3.40		0.947	0.997	5.209	213		
-180	9.761	504	4.76	0.74	0 963	0.98	5 163	232		
-190	9.821	507	2.56		0 964	0.994	5 164	192		
-200	10 23	505	1.73		0.926	0.993	5.181	150		
-210	10.68	510	1.50		0.879	0.994	5.138	128		
-220	10.88	511	1.46		0.855	0.996	5.094	122		
-230	10.39	511	1.62		0.905	0.996	5.133	140		
-240	9.938	512	2.01		0.955	0.996	5.189	169		
-250	9.856	512	3.35		0.960	0.995	5.154	214		
Nozzle C25.0										
39- 30	15.803	462.5	5.00	Uniform	0.952	0.987	7.046	309.2	*	*
- 40	15.801	463 6	3.86		0.952	0.997	7.0414	291.5		
- 50	15.833	465.6	3.26		0.945	1.003	7.028	277.5		
- 60	15.863	466.88	2.60		0.942	1.006	7.0119	253.7		
- 70	15.914	467.6	2.210		0.936	1.003	6.983	232.2		
- 80	16.119	469.4	1.985		0.929	1.002	7.0021	218.4		
- 90	16.294	471.0	1.77		0.913	0.993	7 004	199.6		
-100	16.695	472.3	1.625		0.8977	0.973	6.9905	181.3		
-110	16.326	473.08	1.77		0.909	0.993	6.9724	199.3		
-120	16.155	473.5	2.01		0.926	0.999	6.9665	219.6		
59- 20	17.054	845	7.83	0.646	0.9786	0.95	5.8394	367	1072	720
- 30	17.464	843	4.147	0.646	0.9823	0.987	6.0135	340	1066	718
- 40	17.259	840	2.912	0.643	0.977	0.9895	5.9358	298	1061	716
- 50	17.691	843	2.13	0.646	0.9603	1.009	5.9582	263	1068	716
- 60	18.167	845	1.82	0.643	0.934	1.015	5.947	237	1071	714
- 70	14.466	749	1.62	0.785	0.896	1.00	4.8188	161	936	605
- 80	13.508	751	1.75	0.786	0.921	1.007	4.8509	175	939	606
- 90	13.923	752	1.96	0.784	0.945	1.012	4.8819	193.3	938	608
-100	13.58	753	2.30	0.787	0.957	1.005	4.814	209	938	608
-110	13.418	755	2.66	0.786	0.966	0.9983	4.798	221	942	611
-120	13.515	755	3.265	0.786	0.969	1.000	4.8445	243	945	613
-130	13.40	756	4.32	0.785	0.969	0.985	4.799	259	943	613
-140	12.635	758	6.816	0.783	0.967	0.961	4.7858	281	947	614
59-150	13.529	790	6.78	1.38	0.976	0.937	4.7865	279	1082	561
-160	13.543	793	3.39	1.38	0.976	0.964	4.7855	240	1085	562
-180	13.72	797	2.30		0.965	0.9617	4.839	206	1087	563
-190	14.39	801	1.79		0.9326	0.976	4.834	178	1090	565
-200	13.99	800	1.98		0.95	0.972	4.789	189		
-210	13.70	800	2.675		0.974	0.972	4.809	223		
-220	13.62	802	4.424		0.979	0.9544	4.801	261		
-230	13.60	801	7.00		0.976	0.933	4.783	282		
60- 20	15.94	485	14	0.647	0.960	0.925	7.038	353	*	*
- 30	15.99	486	5.23	0.649	0.956	0.982	7.031	318		
- 40	15.95	488	3.31	0.648	0.958	1.006	7.018	284		
- 50	16.25	489	2.33	0.648	0.949	1.009	7.065	248		
- 60	16.59	491	1.85	0.649	0.921	1.005	6.994	214.0		
- 70	17.42	492	1.60	0.650	0.881	1.0052	7.015	190		
- 80	16.92	493	1.72		0.905	1.0045	6.995	203		
- 90	16.34	493	2.04		0.937	1.0062	6.993	229		
-100	16.03	493	2.60		0.956	1.002	6.993	260		
-110	15.92	494	4.14		0.960	0.9897	6.97	302		
-120	15.92	495	8.33		0.96	0.950	6.97	339		
-130	16.38	496	14.45	1.43	0.936	0.0313	6.987	359		
-140	16.32	496	3.29		1.005	0.9986	6.974	284		
-150	16.55	497	2.37		1.012	1.005	6.995	250		
-160	16.98	498	1.88		1.010	1.002	6.961	216		
-170	17.70	500	1.62		1.009	1.00	6.946	191		
-180	17.33	500	1.74		1.010	1.002	6.959	204		
-190	16.68	501	2.07		1.011	1.003	6.924	230		
-200	16.44	502	2.78		1.011	1.004	6.953	269		
-210	16.37	504	4.05		1.002	0.996	6.941	304		
-220	16.37	505	7.36		0.971	0.965	6.942	339		

*T_{T_p} and $T_{T_B} = T_{T_a}$

.994 .9665 4.958 241.7322

Data Point	P_{T_a}, psia	T_{T_a}, °R	NPR	BPR	C_{DA}	C_{FA}	W_a, lbm/sec	F_a, lbf	T_{Tp}, °R	T_{T_B}, °R
Nozzle C25.1										
40- 20	16.06	460	5.71	Uniform	0.946	0.985	7.242	326	*	*
- 30	16.05	462	4.06		0.946	0.994	7.221	302		
- 40	16.09	463	3.12		0.944	1.004	7.217	280		
- 50	16.20	467	2.66		0.943	1.006	7.231	265		
- 60	16.21	486	2.28		0.939	1.002	7.195	244		
- 70	16.43	469	2.00		0.927	1.003	7.189	225		
- 80	16.46	471	1.88		0.920	0.9961	7.140	213		
- 90	16.51	472	1.88		0.921	0.9971	7.154	215		
-100	16.79	473	1.67		0.903	0.995	7.126	193		
62- 20	13.47	738	6.52	1.36	0.979	0.951	4.967	282	972	555
Case 2 - 30	13.41	757	3.31		0.982	0.962	4.898	238	1033	544
- 40	13.54	766	2.30		0.980	0.963	4.910	206	1048	546
- 50	14.0	771	1.75		0.959	0.958	4.951	172	1055	549
- 60	14.27	769	1.64		0.935	0.962	4.927	162	1052	549
- 70	14.22	773	1.78		0.942	0.979	4.934	178	1056	552
- 80	13.70	774	1.98		0.969	0.967	4.884	189	1056	552
- 90	13.53	774	2.31		0.986	0.960	4.910	206	1061	552
-100	13.42	776	2.78		0.993	0.956	4.899	224	1061	555
-110	13.49	778	4.51		0.996	0.947	4.937	263	1062	556
-130	14.02	766	1.79	0 86	0.924	1.004	4.795	178	974	607
-140	13.66	761	1.96		0.936	1.009	4.750	189	964	605
Case 1 -150	13.38	760	2.61		0.953	1.006	4.737	219	964	606
-160	13.43	762	5.01		0.958	0.9874	4.773	278	965	607
-170	13.43	762	3.4		0.958	1.004	4 771	244	965	607
Nozzle C25.3										
52- 40	15.86	481	2.26	Uniform	0.956	1.006	7.085	243	*	*
- 50	15.97	482	1.79		0.949	0.999	7.075	207		
- 60	15.82	483	5.21		0.96	0.984	7.074	320		
- 70	15.84	484	3.81		0.957	1.00	7.061	298		
- 80	15.84	484	3.07		0.956	1.006	7.052	278		
- 90	15.84	485	2.58		0.958	1.007	7.057	260		
-100	15.83	486	2.27		0.957	1.0077	7.048	243		
-110	15.86	487	2.0		0.954	1.006	7.027	225		
-120	15.94	488	1.78		0.949	0.9987	7.017	205		
-130	16.20	488	1.61		0.936	0.993	7.030	187		
-140	15.85	490	5.20		0.958	0.9872	7.033	321		
-150	15.85	490	3.08		0.956	1.007	7.020	280		
-160	15.83	490	2.22		0.956	1.009	7.002	241		
-170	15.97	492	1.79		0.949	1.002	7.006	208		
66- 20	14.47	723	7.13	1.16	0.986	0.950	5.444	311	961	532
- 30	14.37	729	3.63	1.17	0.992	0.980	5.416	271	964	540
- 40	14.36	731	2.35	1.14	0.987	0.99	5.384	229	968	538
- 50	14.31	733	2.05	1.16	0.988	0.9882	5.361	211	968	542
- 60	14.29	733	1.91	1.13	0.986	0.981	5.348	199	975	540
- 70	14.29	735	2.17	1.19	0.979	0.9925	5.296	217	971	543
- 80	14.32	734	2.93	1.18	0.98	0.993	5.319	251	970	544
- 90	14.07	738	4.83	1.16	0.985	0.969	5.236	283	975	544
-100	12.08	500	5.70	1.16	0.953	0.989	5.280	249	*	*
-110	12.03	500	6.06	1.17	0.961	0.979	5.303	251		
-120	11.98	501	3.03	1.18	0.955	1.011	5.241	211		
-130	12.19	501	2.01	1.16	0.948	1.02	5.297	175		
-140	12.12	502	1.78	1.17	0.941	1.007	5.219	157		
-150	12.42	502	1.64	1.16	0.923	1.01	5.245	147		
-160	12.34	504	1.88	1.18	0.937	1.027	5.283	168		
-170	12.11	503	2.36	1.18	0.951	1.017	5.264	191		
-180	12.10	504	3.96	1.16	0.955	1.005	5.283	231		
-190	11.98	504	5.94	0.73	0.965	0.985	5.275	251		
-200	11.91	504	2.99	0.71	0.973	1.009	5.287	212		
-210	11.90	507	1.99	0.72	0.972	1.009	5.269	172		
-220	12.04	507	1.73	0.72	0.954	1.009	5.229	154		
-230	12.17	507	1.66	0.74	0.942	1.012	5.219	149		
-240	11.99	508	1.81	0.73	0.955	1.011	5.209	160		
Nozzle C25D3										
38- 20	15.63	455	4.87	Uniform	0.948	0.993	7.248	316	*	*
- 30	15.59	457	3.77		0.948	0.998	7.217	295		
- 40	15.69	458	3.20		0.947	1.00	7.243	281		
- 50	15.73	459	2.55		0.945	0.996	7.224	256		
- 60	15.74	459	2.25		0.947	0.986	7.261	238		
- 70	15.65	460	1.98		0.947	0.974	7.208	216		
-100	15.72	462	1.77		0.946	0.965	7.220	198		
-110	15.77	462	1.95		0.947	0.975	7.248	215		
-120	15.77	463	2.22		0.947	0.983	7.244	235		
-130	15.75	463	2.56		0.945	0.994	7.222	256		
-140	15.72	464	3.25		0.945	1.00	7.203	283		
-150	15.80	464	3.96		0.944	1.00	7.227	302		
-160	15.76	464	5.33		0.945	0.992	7.218	324		
67- 60	14.21	744	7.5	1.20	0.96	0.964	5.224	310	992	536
- 70	14.26	744	3.38	1.20	0.96	0.992	5.235	262	991	536
- 80	14.26	743	2.34	1.21	0.958	0.982	5.234	222	989	536
- 90	14.15	744	1.99	1.22	0.957	0.966	5.183	196	989	536
-100	13.65	499	6.08	0.62	0.946	1.003	6.026	292	*	*

Data Point	P_{T_a}, psia	T_{T_a}, °R	NPR	BPR	C_{DA}	C_{FA}	W_a, lbm/sec	F_a, lbf	T_{T_P}, °R	T_{T_B}, °R
					Nozzle C25D3					
67-110	13.58	500	3.41	0.61	0.953	1.015	6.037	254	*	*
-120	13.60	500	2.26	0.61	0.949	1.009	6.023	211		
-130	13.64	501	1.93	0.62	0.951	0.992	6.047	190		
-140	14.00	502	6.10	1.21	0.926	1.004	6.039	294		
-150	14.02	505	3.41	1.22	0.926	1.019	6.037	256		
-160	14.09	505	2.29	1.22	0.929	1.005	6.077	215		
-170	13.99	504	1.96	1.22	0.925	0 9902	6.009	191		
					Nozzle C40.1					
41- 70	16.27	472	2.31	Uniform	0.926	0.9989	5.1767	176	*	*
- 80	16.46	474	2.04		0.921	0.9925	5.202	164		
- 90	16.62	475	1.87		0.911	0.9848	5.186	154		
-100	16.87	476	1.68		0.897	0.960	5.178	136		
-110	16.68	477	1.85		0.912	0.9828	5.198	153		
-120	16.45	478	2.068		0.9206	0.9945	5.177	166		
-130	16.34	479	2.355		0.9318	1.002	5.196	180		
-140	16.25	478	2.72		0.9356	1.006	5.192	194		
-160	16.18	479	3.97		0.934	0.9987	5.155	219		
-170	16.19	480	5.283		0.937	0.985	5.170	231		
-180	16.15	481	6.629		0.938	0.97	5.161	242		
-190	16.16	481	4.53		0.939	0.9898	5.163	226		
-210	16.19	483	3.06		0.937	1.003	5.162	202		
-220	16.28	483	2.51		0.934	1.001	5.167	185		
-230	16.38	483	2.26		0.930	0.9968	5.159	175		
-240	16.61	483	1.91		0.907	0.9921	5.122	156		
-250	16.74		1.79		0.905	0.9756	5.145	147		
57- 20	15.95	481	7.4	0.81	0.945	0.960	5.133	243		
- 30	15.94	484	3.89		0.943	0.995	5.098	215		
- 40	15.99	486	2.56		0.940	1.003	5.087	186		
- 80	16.17	490	2.26		0 93	1.0073	5.071	175		
- 90	16.01	490	3.05		0.94	1.003	5.074	200		
-100	15.94	492	5.49		0.943	0.981	5.055	232		
-110	16.05	494	5.93	1.37	0.936	0.974	5.051	235		
-120	16.04	494	3.90		0.934	0.995	5.035	215		
-130	16.14	495	2.65		0.932	1.002	5.065	189		
-200	16.28	500	2.29		0.923	1.003	5.019	176		
-210	16.03	499	3.14		0.933	0.999	5.000	200		
-220	16.02	501	5 2		0.936	0.982	5 005	229		
					Nozzle SPAC					
47- 30	11.19	466	6.14	Uniform	0.965	0.93	7.130	310	*	*
- 40	11.19	468	3.79		0.965	0.916	7.120	271		
- 50	11.21	469	2.91		0.962	0.872	7.102	234		
- 60	11.25	469	2.35		0.957	0.891	7.091	217		
- 70	11.30	471	1.93		0.955	0.854	7.090	185		
- 80	11.31	471	1.63		0.957	0.834	7.109	159		
- 90	11.28	472	11.92		0.956	0.937	7.073	350		
-100	11.27	473	5.46		0.958	0 930	7.082	303		
-110	11.29	473	2.91		0.954	0.90	7.061	242		
-120	11.35	474	2.27		0.953	0.884	7.079	212		
-130	11.36	476	1.94		0.953	0.863	7.077	189		
-140	11.43	476	1.64		0 946	0.808	7.068	154		
-150	11.27	477	1.51		0.958	0 836	7.050	147		
					Nozzle UPAC					
45- 30	15.96	476	5.32	Uniform	0.959	0.95	4.768	207	*	*
- 40	15.94	477	3.97		0.958	0.935	4.754	189		
- 50	15.93	478	3 38		0.959	0.961	4.751	184		
- 70	15.95	478	2.38		0.958	0.988	4.753	164		
- 80	15.99	478	2.02		0.95	0.989	4.724	148		
- 90	16.28	478	1.81		0.936	1.043	4.739	145		
-100	16.54	479	1.73		0.922	1.009	4.739	135		
-110	15.93	480	5.19		0.952	0 958	4.710	206		
-120	15.92	481	4.18		0.957	0.961	4 722	196		
-130	15.94	481	3 20		0.958	0.972	4.735	183		
-140	15.93	481	2.72		0.956	0.992	4.722	175		
-150	16.00	482	2.32		0.956	0.991	4.738	162		
-160	15.96	482	2.07		0.954	0.993	4 713	152		
-170	16.31	482	1.85		0.936	1.002	4.727	142		
-180	16.73	482	1.68		0.911	1 026	4.716	134		
50- 30	18 86	749	26.53	0 864	0.958	0 962	4.487	315	927	659
- 40	18.85	752	4.43	0.866	0.963	0.983	4.503	244	928	662
- 50	18 88	751	3 08	0.866	0.962	0.975	4.504	215	929	660
- 60	18.92	751	2 31	0.867	0.959	1.024	4.501	199	931	659
- 70	19 18	750	1 88	0.867	0 943	1.028	4.489	175	927	659
- 80	18.90	752	2.12	0 865	0 957	1.028	4.484	189	931	660
- 90	18 81	754	2 67	0.869	0 963	1.014	4 485	211	935	662
-100	18 79	754	3 49	0.871	0.962	0.994	4.477	228	934	662
-110	18.78	755	5 87	0.869	0 966	0.993	4.490	263	931	665
-130	20.58	787	3.3	1.40	0.997	0.983	4.977	252	1050	631
-140	20.53	781	2 55	1.50	0.995	1.004	4.985	231	1039	626
-170	20 61	780	2.86	1 49	0.993	0.999	4.980	241	1039	624
-180	20 63	781	4.01	1.49	0.993	0 975	4.986	278	1038	626
-190	20.60	781	4.85	1.49	0.993	0.97	4.981	277	1038	626

APPENDIX B
NOZZLE TOTAL PRESSURE AND TOTAL TEMPERATURE PROFILES

C15.1 Nozzle

Data Point 64-90, BPR = 3.89, BTR = 0.547, NPR = 3.89

r/r_w	-0.80	-0.69	-0.55	-0.41	0	0.19	0.33	0.43	0.57	0.71	0.85	1.0
P_T, psia	11.60	11.69	12.04	12.11	12.10	12.10	12.07	12.03	11.91	11.72	11.63	11.62
T_T, °R	541	678	904	981	988	987	982	976	931	755	540	539

Data Point 64-170, BPR = 1.28, BTR = 1.0, NPR = 3.40

r/r_w	-0.80	-0.69	-0.55	-0.41	0	0.19	0.33	0.43	0.57	0.71	0.85	1.0
P_T, psia	10.30	9.96	9.70	9.71	9.67	9.66	9.66	9.68	9.62	9.84	10.37	10.37
T_T, °R	505											

Data Point 64-250, BPR = 0.74, BTR = 1.0, NPR = 3.35

r/r_w	-0.80	-0.69	-0.55	-0.41	0	0.19	0.33	0.43	0.57	0.71	0.85	1.0
P_T, psia	9.43	9.86	10.28	10.39	10.40	10.39	10.36	10.30	10.13	9.71	9.43	9.43
T_T, °R	512											

C25.0 Nozzle

Data Point 59-40, BPR = 0.64, BTR = 0.675, NPR = 2.91

r/r_w	-0.80	-0.69	-0.55	-0.41	0	0.19	0.33	0.43	0.57	0.71	0.85	1.0
P_T, psia	16.32	17.34	18.18	18.53	18.58	18.57	18.48	18.47	18.21	16.89	16.22	16.21
T_T, °R	700	815	898	1028	1061	1060	1054	1028	922	777	716	716

Data Point 59-120, BPR = 0.786, BTR = 0.650, NPR = 3.27

r/r_w	-0.80	-0.69	-0.55	-0.41	0	0.19	0.33	0.43	0.57	0.71	0.85	1.0
P_T, psia	12.97	13.55	14.05	14.26	14.23	14.23	14.20	14.18	13.98	13.37	12.95	12.95
T_T, °R	613	763	869	939	945	944	941	932	880	710	613	612

Data Point 59-160, BPR = 1.38, BTR = 0.518, NPR = 3.39

r/r_w	-0.80	-0.69	-0.55	-0.41	0	0.19	0.33	0.43	0.57	0.71	0.85	1.0
P_T, psia	13.51	13.43	13.63	13.67	13.62	13.62	13.60	13.58	13.57	13.47	13.52	13.53
T_T, °R	573	802	992	1083	1085	1084	1079	1072	1014	706	562	562

C25.0 Nozzle

Data Point 60-40, BPR = 0.65, BTR = 1.0, NPR = 3.31

r/r_w	-0.80	-0.69	-0.55	-0.41	0	0.19	0.33	0.43	0.57	0.71	0.85	1.0
P_T, psia	15.44	15.99	16.50	16.66	16.66	16.66	16.64	16.60	16.42	15.79	15.39	15.39
T_T, °R	486											

Data Point 60-210, BPR = 1.43, BTR = 1.0, NPR = 4.05

r/r_w	-0.80	-0.69	-0.55	-0.41	0	0.19	0.33	0.43	0.57	0.71	0.85	1.0
P_T, psia	16.79	16.19	15.93	15.92	15.88	15.88	15.86	15.87	15.89	16.37	16.89	16.89
T_T, °R	504											

C25.1 Nozzle

Data Point 62-30, BPR = 1.36, BTR = 0.527, NPR = 3.31

r/r_w	-0.80	-0.69	-0.55	-0.41	0	0.18	0.33	0.43	0.57	0.71	0.85	1.0
P_T, psia	13.32	13.35	13.48	13.53	13.55	13.55	13.45	13.48	13.45	13.31	13.36	13.37
T_T, °R	544	779	938	1024	1033	1033	1024	1020	966	677	544	544

Case 2

Data Point 62-150, BPR = 0.86, BTR = 0.629, NPR = 2.61

r/r_w	-0.80	-0.69	-0.55	-0.41	0	0.18	0.33	0.43	0.57	0.71	0.85	1.0
P_T, psia	12.93	13.49	13.86	13.96	13.96	13.95	13.93	13.90	13.77	13.23	12.92	12.92
T_T, °R	604	777	883	958	964	964	959	951	904	715	603	603

Case 1

C25.3 Nozzle

Data Point 66-80, BPR = 1.18, BTR = 0.56, NPR = 2.93

r/r_w	-0.79	-0.69	-0.55	-0.41	0	0.19	0.34	0.43	0.57	0.71	0.85	1.0
P_T, psia	14.06	14.25	14.52	14.57	14.60	14.61	14.62	14.52	14.44	14.17	14.20	14.20
T_T, °R	560	752	901	971	970	970	963	961	915	660	543	543

Data Point 66-200, BPR = 0.71, BTR = 1.0, NPR = 2.99

r/r_w	-0.79	-0.69	-0.55	-0.41	0	0.19	0.34	0.43	0.57	0.71	0.85	1.0
P_T, psia	11.69	12.13	12.28	12.22	12.36	12.35	12.41	12.31	12.13	11.82	11.47	11.47
T_T, °R	506											

C25D3 Nozzle

Data Point 67-70, BPR = 1.19, BTR = 0.54, NPR = 3.38

r/r_w	-0.83	-0.69	-0.54	-0.40	0	0.20	0.34	0.43	0.58	0.71	0.86	1.0
P_T, psia	14.09	14.18	14.54	14.56	14.48	14.47	14.47	14.46	14.36	14.16	14.08	14.08
T_T, °R	535	696	934	990	991	990	985	977	920	739	535	535

Data Point 67-110, BPR = 0.614, BTR = 1.0, NPR = 3.41

r/r_w	-0.83	-0.69	-0.54	-0.40	0	0.20	0.34	0.43	0.58	0.71	0.86	1.0
P_T, psia	12.99	13.58	14.24	14.37	14.31	14.31	14.31	14.19	14.14	13.04	12.93	12.93
T_T, °R	500	→										

Data Point 67-150, BPR = 1.23, BTR = 1.0, NPR = 3.41

r/r_w	-0.83	-0.69	-0.54	-0.40	0	0.20	0.34	0.43	0.58	0.71	0.86	1.0
P_T, psia	14.27	13.92	13.78	13.79	13.79	13.79	13.76	13.75	13.79	13.94	14.35	14.36
T_T, °R	505	→										

C40.1 Nozzle

Data Point 57-90, BPR = 0.81, BTR 1.0, NPR = 3.05

r/r_w	-0.82	-0.73	-0.50	-0.37	0	0.22	0.35	0.47	0.61	0.75	0.89	1.0
P_T, psia	15.81	16.01	16.17	16.17	16.20	16.20	16.23	16.17	16.13	15.84	15.86	15.86
T_T, °R	489	490	490	490	489	490	490	489	491	490	492	492

Data Point 57-210, BPR = 1.36, BTR = 1.0, NPR = 3.14

r/r_w	-0.82	-0.73	-0.50	-0.37	0	0.22	0.35	0.47	0.61	0.75	0.89	1.0
P_T, psia	16.41	15.99	15.92	15.87	15.88	15.88	15.91	15.86	15.88	16.30	16.29	15.70
T_T, °R	499	499	499	499	500	500	500	500	499	498	500	500

UPAC Nozzle

Data Point 56-50, BPR = 0.87, BTR = 0.71, NPR = 3.08

r/r_w	-0.72	-0.59	-0.46	-0.37	-0.23	0	0.27	0.39	0.58	0.64	0.87	1.0
P_T, psia	18.77	18.92	19.16	19.25	19.27	19.28	19.32	19.30	19.16	18.99	18.58	18.58
T_T, °R	714	759	815	865	929	930	968	908	784	759	662	660

Data Point 56-180, BPR = 1.49, BTR = 0.60, NPR = 4.01

r/r_w	-0.72	-0.59	-0.46	-0.37	-0.23	0	0.27	0.39	0.58	0.64	0.87	1.0
P_T, psia	20.58	20.63	20.63	20.67	20.72	20.72	20.76	20.77	20.67	20.72	20.58	20.58
T_T, °R	738	818	906	969	1034	1038	1080	1024	848	796	626	625

NOMENCLATURE

A	Cross-sectional area
BPR	Bypass mass flow ratio, W_B/W_P
BTR	Bypass Temperature Ratio, T_{TB}/T_{TP}
C_D	Discharge coefficient
C_{DA}	Area-weighted discharge coefficient, defined by Eq. 3
C_{DS}	Radially weighted discharge coefficient defined by Eq. 4
C_F	Thrust coefficient
C_{FA}	Area-weighted thrust coefficient, defined by Eq. 6
C_{FS}	Radially weighted thrust coefficient defined by Eq. 7
D	Diameter
F	Force (or thrust)
g	Standard g_c conversion factor between $\#_F$ & $\#_m$
L	Length
M	Mach number
NPR	Nozzle pressure ratio
n	Number of stream tube elements
P	Static pressure
P_T	Total pressure
R	Gas constant
$R_c{}^*$	Nozzle lip radius of curvature normalized by throat radius

r	Radial distance from nozzle centerline
T	Static temperature
T_T	Total temperature
u	Axial velocity component
W	Mass flow rate
X	Axial distance from nozzle throat (positive in downstream direction)
α	Flow angle
γ	Ratio of specific heats
Δ	Small increment
δ^*	Boundary layer displacement thickness
ρ	Density
τ_w	Wall shear force

SUBSCRIPTS

1-D	One dimensional
a	Actual
B	Bypass
bl	Boundary layer
c	Cell
cb	Centerbody (or axis)
e	Exit
f	Final

i	Initial
P	Primary or core flow
w	Outer wall
∞	Free stream

SUPERSCRIPTS

*	Throat plane
A	Area weighted
S	Radially segmented